machines

MDPI

Article

Design and Performance of a Novel Tapered Wing Tiltrotor UAV for Hover and Cruise Missions

Edgar Ulises Rojo-Rodriguez [1], Erik Gilberto Rojo-Rodriguez [1] and Sergio A. Araujo-Estrada [2] and Octavio Garcia-Salazar [1,*]

[1] Aerospace Engineering Research and Innovation Center, Faculty of Mechanical and Electrical Engineering, Autonomous University of Nuevo Leon, Apodaca 66616, Nuevo Leon, Mexico; edgar.rojordrg@uanl.edu.mx (E.U.R.-R.); erojor@uanl.edu.mx (E.G.R.-R.)

[2] Department of Aeronautical and Astronautical Engineering, University of Southampton, Southampton SO16 7PX, UK; s.araujo-estrada@soton.ac.uk

* Correspondence: octavio.garciasl@uanl.edu.mx

Abstract: This research focuses on a novel convertible unmanned aerial vehicle (CUAV) featuring four rotors with tilting capabilities combined with a tapered form. This paper studies the transition motion between multirotor and fixed-wing modes based on the mechanical and aerodynamics design as well as the control strategy. The proposed CUAV involves information about design, manufacturing, operation, modeling, control strategy, and real-time experiments. The CUAV design considers a fixed-wing with tiltrotors and provides the maneuverability to perform take-off, hover flight, cruise flight, and landing, having the characteristics of a helicopter in hover flight and an aircraft in horizontal flight. The manufacturing is based on additive manufacturing, which facilitates the creation of a lattice structure within the wing. The modeling is obtained using the Newton–Euler equations, and the control strategy is a PID controller based on a geometric approach on SE(3). Finally, the real-time experiments validate the proposed design for the complete regime of flight, and the research meticulously evaluates the feasibility of the prototype and its potential to significantly enhance the mission versatility.

Keywords: convertible UAV; tilting rotors; manufacturing; design; real-time experiments

check for updates

Citation: Rojo-Rodriguez, E.U.; Rojo-Rodriguez, E.G.; Araujo-Estrada, S.A.; Garcia-Salazar, O. Design and Performance of a Novel Tapered Wing Tiltrotor UAV for Hover and Cruise Missions. *Machines* **2024**, *12*, 653. https://doi.org/10.3390/machines12090653

Academic Editors: Giuseppe Carbone and Luca Bruzzone

Received: 17 June 2024
Revised: 5 August 2024
Accepted: 9 September 2024
Published: 18 September 2024

Copyright: © 2024 by the authors. Licensee MDPI, Basel, Switzerland. This article is an open access article distributed under the terms and conditions of the Creative Commons Attribution (CC BY) license (https://creativecommons.org/licenses/by/4.0/).

1. Introduction

In recent years, unmanned aerial vehicles (UAVs) have become increasingly common in several civilian and military applications, including search and rescue, highway patrol, and inspecting infrastructure such as power lines, bridges, factories, buildings, exteriors, sewers, railroads, and wind turbines. There exist three main types of UAVs: multirotors, airplanes, and convertible UAVs (non-conventional configurations) [1].

The take-off and landing have historically presented difficulties for UAVs because of the limitations involved in each different configuration. In this sense, a fixed-wing UAV presents high aerodynamic performance and requires a runway in order to take off and land; however, a rotary-wing UAV suffers performance limitations in terms of endurance, range, and maximum forward speed. In order to combine these capabilities of the fixed-wing and rotary-wing UAVs, a solution is proposed in this paper: a tiltrotor configuration with a tapered wing.

Classic fixed-wing vehicles require dedicated runway infrastructure, limiting their operational reach [2]. Convertible aircrafts, on the other hand, can operate from confined spaces and eliminate the need for extensive runways. This translates to increased accessibility for remote locations, urban environments, and disaster zones where traditional landing strips might be unavailable or damaged [3]. While offering vertical agility similar to helicopters, convertible vehicles can transition to fixed-wing flight for extended range and

higher cruise speeds compared to rotary-wing vehicles. This provides a significant advantage in terms of operational efficiency, particularly for applications such as long-distance cargo delivery, search and rescue missions over vast areas, or border patrol activities [4].

Research on convertible UAVs requires knowledge of rotary-wing and fixed-wing vehicles to combine hover and cruise flight properties; it means a CUAV that performs a complete flight: take-off, hover, cruise, and landing modes. Some convertible UAVs can be found in [5], computational fluid dynamics (CFD) simulation and aerodynamic characterization in [6], flight dynamics modeling and stabilization in [7], and additionally, the tilting mechanism was designed in [8]. The development of convertible vehicles, tiltrotor UAVs, tilt-wing UAVs, tail-body or tailsitter UAVs, has garnered significant interest in the scientific community [9–11]. The domain of convertible UAV indexing presents a multifaceted landscape. While a multitude of researchers have opted for bespoke designs with unique implementation strategies, this very diversity creates a significant challenge for comprehensive study. Nonetheless, several prominent approaches hold particular significance and warrant mention within the relevant literature. These approaches include a tiltrotor convertible UAV involving a quad-rotor design equipped with a tilting mechanism, as addressed in [12]. This mechanism provides the ability to dynamically change the direction of propulsion. This vehicle was stabilized with a nonlinear control for the complete regime of flight, and the autopilot was developed using a low-cost DSP embedded system to achieve real-time experiments. A prototype employing vectorized thrust was presented in [13], enabling the capability for motion without the need for corresponding body movement. This algorithm was validated in real-time experiments, showing the effectiveness of the proposed controller. In [14], the development of the transitioning vehicle called Cyclone was proposed, whose mission is to perform hover and horizontal flights considering a control with incremental nonlinear dynamic inversion. The real tests demonstrated the vertical take-off and landing capabilities of the vehicle. Furthermore, research on lightweight materials is crucial to optimize performance and range [15,16]. These advancements can have a ripple effect, benefiting the development of future generations of both conventional and unconventional aircraft.

In [17], a flight control system of a small tiltrotor UAV was proposed, and it is based on an improved mathematical model. The proposed controller is based on an eigenstructure assignment, and the proposed approach has been validated in a wind tunnel test and real-time flights. In [18], the authors presented a methodology to design a tiltrotor microair vehicle in order to perform hovering and cruise flight scenarios. Results showed the aerodynamic parameters of the proposed vehicle. The authors in [19] proposed a geometrically compatible integrated design to develop for the conformal rotor and nacelle of the distributed propulsion tilt-wing UAV. This methodology considered the complex geometric constraints and coordinated the aerodynamic efficiency of the rotor and nacelle, allowing a low drag. A tiltrotor UAV was presented in [20] whose configuration drives the attitude based on tilting rotors. The control strategy is based on a bounded smooth function, and it was implemented in real-time flights. In [21], a small trirotor test bed with tilting propellers was proposed to validate the flight control laws. The controller algorithm is based on a nonlinear dynamic inversion with two layers. The lower layer involves attitude stabilization, while the higher layer manages trajectory tracking. The authors in [22] worked on a robust adaptive mixing controller to achieve the trajectory tracking of a quad-tiltrotor convertible plane, and the mathematical model is obtained using Euler–Lagrange formalism. To validate the controller, the authors executed hardware-in-the-loop experiments. In [23], a model predictive controller was proposed for tiltrotor UAVs demonstrating the performance in real-time flights. The controller strategy considered a control allocation algorithm, and the model predictive control constitutes a unified nonlinear control for the convertible UAV that performs the complete flight. In [24], the authors presented a CFD (computational fluid dynamics) simulation for a tiltrotor UAVs in order to examine the flow fields on the fuselage and rotor under the transition mode of the vehicle. A transition strategy design based on optimization methods was proposed in [25];

the transition problem is solved using the optimal method with nonlinear programming. The optimization results showed that the transition strategy can manage the relationship between transition time, control input, and attitude stability. The work in [26] proposed a multidisciplinary optimization algorithm for preliminary convertible UAV design. This design is based on aerodynamic models, and it is validated using optimization techniques. Ref. [27] presented the design of a convertible UAV considering the parameters of the rotor, propeller, wing, and airfoil selection. The CUAV design was based on a flying wing and modified to add the tilting rotors. A basic PID controller was tested in real-time. In [28], the authors focus on a controller based on an MPC-based position for a tiltrotor tricopter VTOL UAV. The controller involves a conventional control in the outer loop, while the inner loop is an MPC controller. The simulation was executed for trajectory tracking under the realistic actuator limits. However, our proposed vehicle differs from those published in the literature, since it involves tiltrotor mechanisms combined with a tapered wing; in hover flight, the vehicle is controlled via the propulsion system providing vertical lifting acting against the gravity field. In horizontal mode, the convertible vehicle is airborne, so that the outer body surface (tapered wing) provides the lift force to maintain the horizontal flight.

The main contribution of this paper is a novel convertible tiltrotor UAV using a tapered wing in order to perform a hover flight as a helicopter and a horizontal flight as an airplane. The methodological process is outlined to achieve a comprehensive design to address the convertible configuration as well as the interaction between manufacturing and flight computer development. Real-time experiments are performed to validate system behaviors. The contribution of this paper is summarized as follows:

1. Development of a novel tapered wing tiltrotor UAV for hover and cruise missions.
2. A scheme of guidance, navigation, and control based on the special Euclidean group SE(3) for the convertible UAV.
3. The proposed convertible UAV is tested to obtain the performance in real-time flights.

The rest of this paper is organized as follows. Section 2 presents information about the UAV configuration, operational functions, performance, and manufacturing. Section 3 describes the equations of motion for the convertible UAV using the Newton–Euler formulation and proposes the geometric navigation based on the special Euclidean group SE(3) with a guidance frame and a saturated PID control. Section 4 presents the experimental platform and the autonomous navigation results of the convertible UAV. Finally, conclusions are given in Section 5.

2. Design Proposal

This section outlines a comprehensive design proposal for a convertible unmanned aerial vehicle (UAV) aimed at addressing the flight mission for both hover flight and cruise flight. Our proposal is motivated by the ever-increasing demand for versatile UAV systems capable of dynamically adapting to diverse and complex mission requirements. The subsequent sections address the configuration, actuation, manufacturing, and performance, elucidating the challenges encountered in the development and deployment and presenting significant potential for expanding the capabilities of UAVs. Figure 1 shows the schematic of the proposed convertible UAV and the operation efficiently under various flight conditions.



Figure 1. UAV mission proposal over different areas.

2.1. UAV Configuration

The proposed UAV configuration plays a pivotal role in its adaptability and flight capabilities. The main feature of this configuration is the use of frontal rotors with tilting capabilities and the rear rotor with a coaxial mechanism providing sufficient lift in the hover flight while the wing is a T-shaped design providing the lift force in the forward flight.

The frontal tiltrotors enable the UAV to transition seamlessly and continuously between hover and cruise modes, as shown in Figure 2. During take-off and hover, the rotors are oriented vertically, providing the necessary lift and control (right side of Figure 2). As the UAV transitions to forward flight, the rotors tilt horizontally, allowing the fixed wing to generate lift in relation to airspeed (left side of Figure 2). This dynamic configuration offers the best of both modes, combining the agility and versatility of a multirotor with the efficiency and endurance of a fixed-wing aircraft.

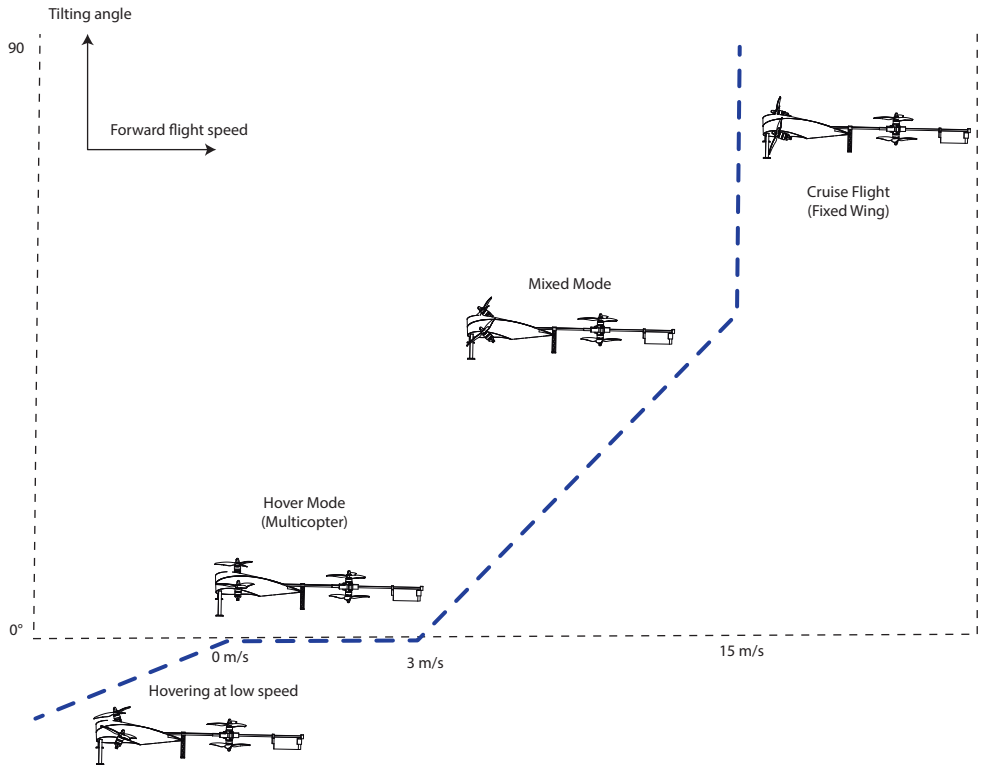


Figure 2. Flight phases for convertible UAV.

The T-shaped distribution of the frontal rotors ensures stability and control during the transition phase and fixed-wing flight. This configuration optimizes the UAV aerodynamic properties and reduces drag, improving performance and energy efficiency. Following this convention, the proposed configuration, as shown in Figure 3, involves the entire array of propulsion and structural fuselage.

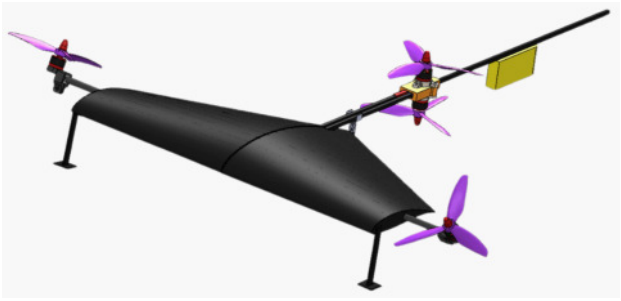


Figure 3. Proposal of the convertible UAV.

2.2. Physical Parameters

This section presents the physical parameters of the platform, detailing its components in both configurations and highlighting the mechanisms that enable its convertibility. In the context of this convertible UAV design, a total weight estimation is required to reach the hover mode and to facilitate the analysis of the dual operational configuration. The first stage involves a multirotor configuration that supports the vehicle weight and enables flight control. However, the design also necessitates a fixed-wing configuration for forward flight. Consequently, appropriate airfoil selection and subsequent lift generation estimation are crucial considerations. It is important to note that the design is constrained by a maximum volume, with a boundary box of 0.065 m $\times$ 0.070 m $\times$ 0.020 m, to maintain a micro-UAV classification [29]. The proposed parameters are detailed in the Table 1.

Table 1. Aircraft physical parameters.

Parameter	Value
Span	0.04 m
Wing Root	0.024 m
Wing Tip	0.012 m
Wing Surface	0.075 m^2
Frontal Arms Length	0.025 m
C.G. to frontal	0.018 m
C.G. to bottom	0.016 m
Airfoil	FX-63
Incidence Angle	3°
Weight	420 g

These design parameters are chosen with the main objective of minimizing weight and enabling the complete regime of flight. Consequently, a total weight of less than 500 g and a compact volume are prioritized. These parameters significantly contribute to an aircraft maneuverability within a confined environment. Additionally, the wing surface selection process considers the airfoil type and its capacity to generate sufficient lift for sustained forward flight.

Note that equation $n = (L + F_I)/(W)$ presents the relationship between lift force, rotor force, and weight; a factor must be equal to or greater than 1 for the aircraft to fly. Considering load factors, this convertible UAV needs to be designed for two flight

regimes. In multirotor mode, the aircraft is prepared for 4*G* to handle the fast maneuvers needed for stability and precision. However, for fixed-wing mode, the design needs to consider the different load factors experienced during cruise flight. This presents a design challenge for the convertible UAV. The structure needs to be robust enough to withstand $\pm 4G$ accelerations in multirotor mode while also being lightweight for efficient fixed-wing flight. Additionally, the wing design, selected tapered form, of the convertible UAV is optimized for both high lift generation during multirotor operation and efficient aerodynamic performance during fixed-wing flight.

This design is developed based on additive manufacturing (AM) techniques to find lightweight parameters and integrate the entire mechanism into the internal structure, see Table 2. Different materials are used for various groups of parts, considering structural and impact reasons [16], as determined from structural optimization. The system is evaluated under static conditions, as this study focuses on representing maximum structural stress in dynamic environments. It uses maximum thrust for information on the internal structure, which informs optimization and deflection rejection.

Table 2. Materials specifications.

Part	Material
Wing Surface	ABS
Structural Frontal Arm (Left and Right)	Fiber Glass tube
Rotor Adapter	PETG
Tilt Mechanism	HIPS

Multiple studies are performed to develop and validate the effectiveness of geometrical optimization of this model, which is based on AM and also uses Solid Isotropic Material with Penalization (SIMP). SIMP is a powerful optimization algorithm determining the optimal material distribution within a design domain. SIMP generates lightweight structures with enhanced stiffness and strength by iteratively removing material from low-stress regions. When it is combined with 3D printing, this approach enables the fabrication of complex, lattice-like structures that would be infeasible using traditional manufacturing methods [30]. To effectively utilize SIMP optimization, it is essential to couple it with finite element analysis (FEA) and computational fluid dynamics (CFD) simulations. FEA provides accurate predictions of structural behavior under various loading conditions, while CFD enables aerodynamic performance evaluation. Figure 4 shows the mesh definition for the finite element method of the proposed CUAV. By iteratively refining the design based on simulation results, engineers can achieve optimal component performance.

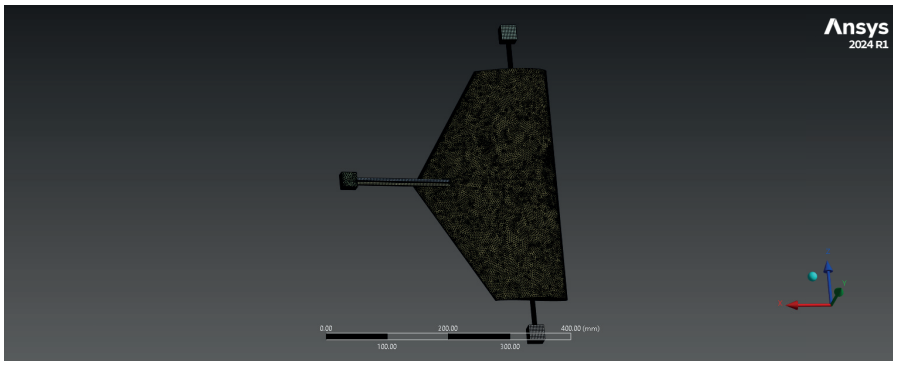


Figure 4. FEM mesh definition.

A maximum input force for thrust force is applied on each rotor base, which is also illustrated in Figure 5; it represents the maximum maneuver allowed by this type of aircraft. The center of gravity is selected as a fixed point for statics study, which is similar to a

ground experiment on deformation effects shown in Figure 6, allowing for a geometrical profile of deformation. In Figure 7) it is shown the forces definition for cruise case. The structure deformation for cruise condition is depicted in Figure 8. A maximum deformation of 0.9258 mm on noncritical parts at the hover phase and 0.2921 mm for the cruise phase since these results are expected due to different forces distribution which is expected on lightweight structures. In this specific case, it is concentrated over the bottom part, which is only affected in hover mode and compensated by the control scheme.

The primary objective of this analysis is to evaluate the deformation characteristics and verify the structural integrity of the model under specified loading conditions. By utilizing ANSYS Mechanical, the objective is to identify potential weaknesses and ensure that the structure can withstand the applied forces without compromising its integrity.

The model created for this study is reduced to a mechanical representation of aircraft in order to simplify the model and develop a mesh of 2.5 mm of element size with a level of 7 at adaptive sizing resolution. These mesh elements were selected due to the minimum element size on the system with a 4.01 mm element, which is covered by the 1.25 mm change on elements selected on configurations.

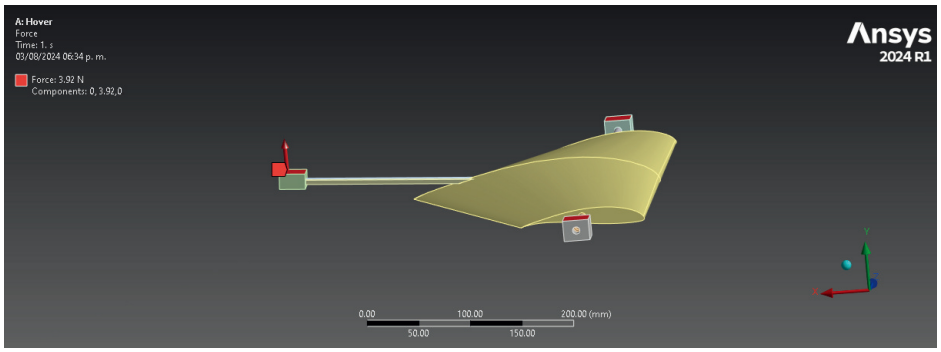


Figure 5. Forces definition for hover case.

For hover conditions, forces are placed at rotor points due to its multirotor nature, as seen in the red zones in Figure 5; for the maximum force developed by the rotor configuration, we selected 3.92 N for each rotor.

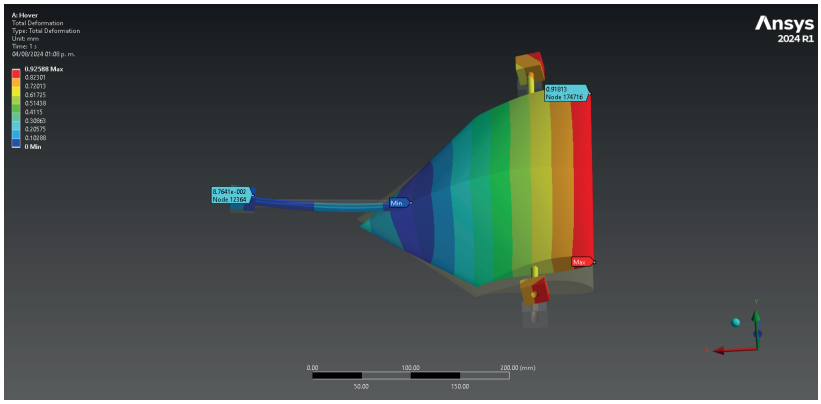


Figure 6. Structure deformation for hover condition.

Considering that the main structure is developed by ABS material and distributed to rotors by fiberglass tubes, it takes account of wing deformation, as shown in Figure 6. It has a probe illustrating the maximum deformation point at the inlet part. This behavior is ideal for this configuration due to the type of manufacture, which demonstrates the effectiveness of SIMP optimization, placing forces at required points. For this geometry, it is used to place internal structures on those points.

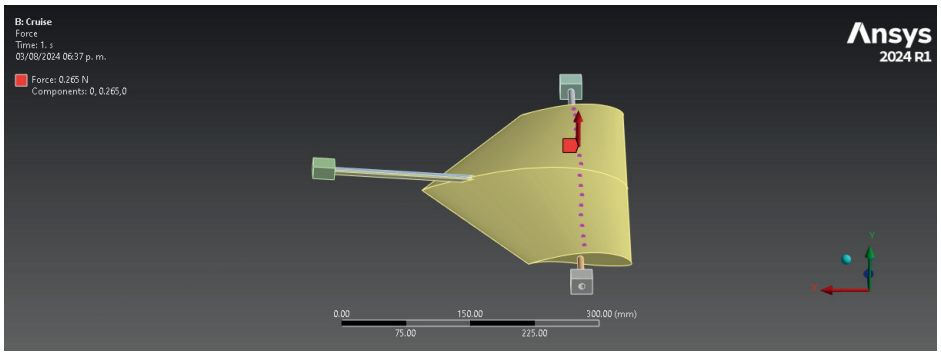


Figure 7. Forces definition for cruise case.

The cruise flight part of the study is used to verify wing effectiveness; in this case, it is developed as a force on a 1/4 part of the wing, which is later demonstrated in the CFD study. Addressing that point, a distribution is selected for force points at the wing surface. Figure 7 includes a distribution of the 14 m/s case, becoming a Gaussian distribution due to this wing geometry, with a total force of 4.24 N, which is the force required to lift the whole aircraft for cruise flight.

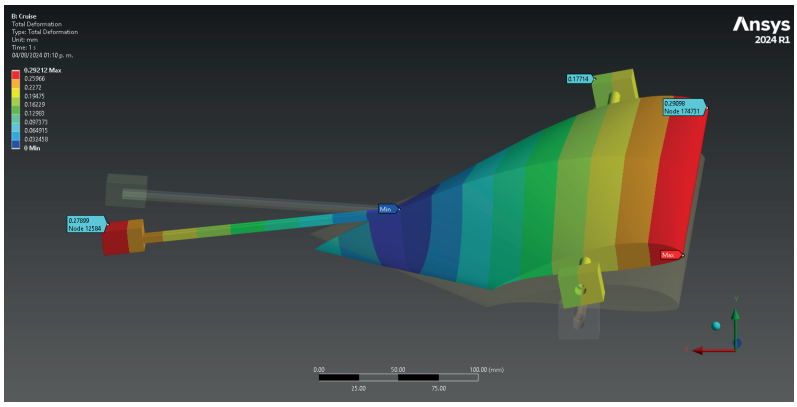


Figure 8. Structure deformation for cruise condition.

Actual results show the value 0.29098 mm as the maximum point of deformation, which is ideal for this micro-UAV case, making a structure that could handle the system and creating a force of 0.17714 mm on the rotor pads, which would not affect the final rotor force vector.

Considering the concentration of deformation shown in Figure 6, it is evident that the frontal rotors would experience the most deformation and equivalent stress, making it a critical point for examination. The frontal arms exhibit a maximum deformation of 0.92 mm under extreme conditions, although such conditions may not occur in real-world scenarios. However, given that these are made of a polymeric material of ABS nature, these can withstand this deformation while maintaining proper operation.

It is important to note that this structure is designed to withstand and exceed forces generated by aerodynamic conditions and rotor forces. This decision ensures the ability to accommodate dynamic behaviors without encountering issues. The accuracy and reliability of CFD simulations heavily depend on the mesh quality used to discretize the computational domain. This study highlights the significance of mesh refinement in capturing the intricate aerodynamic features of a wing. For this case, an adaptive mesh is selected. The outer air domain, which extends 150 mm from the wing, is crucial for capturing the far-field effects of the airflow, as shown in Figure 9. A coarser mesh is sufficient in this region to reduce computational cost while accurately predicting the overall flow behavior. Closer to the wing, within a 500 mm proximity, the mesh is refined to capture the near-field aerodynamic effects more accurately, using a body influence, which affects the 10 mm

element size modification. The wing surface requires a highly refined mesh to capture the boundary layer effects and surface pressure distribution accurately. An element size of 1 mm is employed over the wing surface, which is essential for resolving the fine details of the flow around the wing, including the leading and trailing edges. To capture accurately the boundary layer development, 10 inflation layers are used on the wing surface, which are validated in Figure 10. These layers allow for a gradual transition from the wing surface to the free-stream, ensuring that the viscous effects are well resolved. The first layer of thickness is carefully chosen to capture the near-wall gradients accurately.

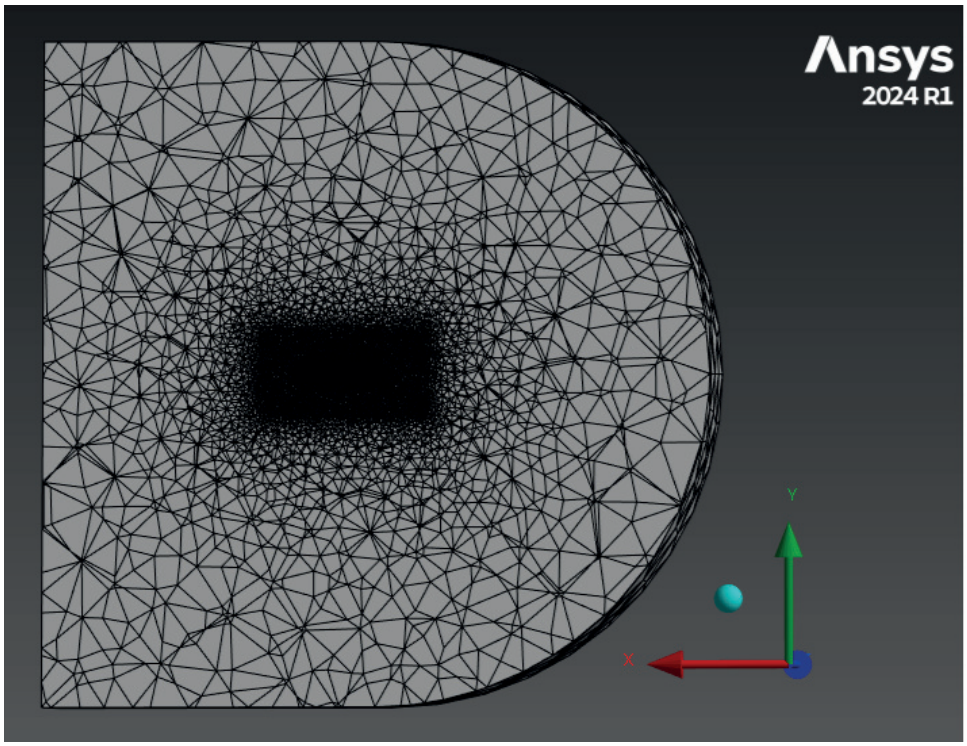


Figure 9. General CFD mesh.

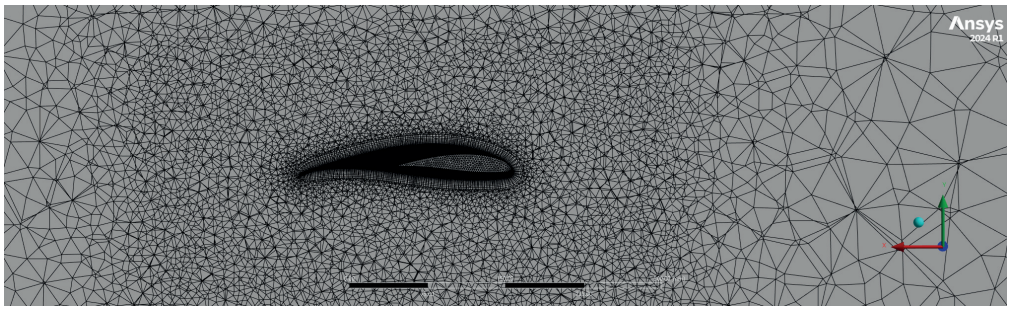


Figure 10. Detailed CFD mesh with the airfoil.

The system is analyzed under various scenarios, particularly at an airspeed of 14 m/s, as shown in Figure 11. It is observed that the system interacts with the air during cruise flights in a similar way to a flying wing thanks to the proposed design. This design minimizes external parts, exposing only the rotors and fixed wing, thus optimizing aerodynamic efficiency.

The CFD analysis employed a high-fidelity model encompassing both the wing and rotor geometries. The simulations are run with an inlet velocity of 14 m/s, representing typical cruise conditions. The selection of the FX63 airfoil for the wing is based on its well-documented performance characteristics.

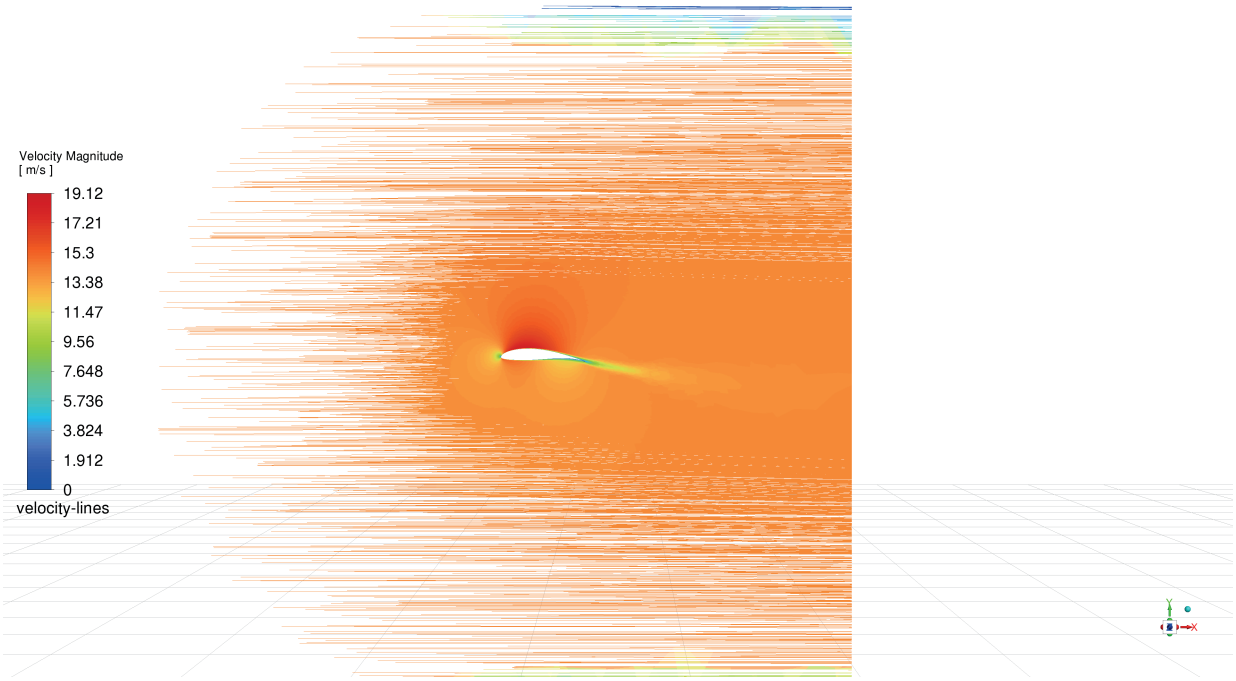


Figure 11. Airflow distribution.

Figure 11 presents contours colored by velocity magnitude, visualizing the flow behavior around the wing. The absence of significant deviations or swirling patterns in the contour suggests a predominantly laminar (non-turbulent) flow regime under the simulated conditions.

Furthermore, the analysis reveals that the airfoil design effectively accelerates the incoming flow. The velocity magnitude increases from the initial 14 m/s at the inlet to approximately 36 m/s over the wing surface. This acceleration is crucial for generating lift, which is a vital force for flight.

Understanding pressure gradients is vital for identifying regions of flow separation and potential stall. This information is crucial for designing airfoils that maintain smooth airflow, enhancing the performance and stability of the UAV; for that reason, it is analyzed in Figure 12. Pressure distribution data are essential for structural analysis. It helps determine the aerodynamic loads acting on the airfoil, which is necessary for ensuring the structural integrity and durability of the UAV. The CFD results reveal detailed pressure contours and distributions over the FX63-137 airfoil. High-pressure regions on the lower surface and low-pressure regions on the upper surface indicate the generation of lift. Areas of adverse pressure gradients highlight potential regions for flow separation, providing insights into the stall characteristics of the airfoil.

Multiple CFD studies were performed, and more prominent results are presented in Table 3, which mention different scenarios of this aircraft. The ideal scenario for this design is design point (DP) 9, where the aircraft flight is stable at the cruise case, considering that 3° is the incidence angle developed for this design.

Other cases are also analyzed as high angles of DP 10–13, showing that this aircraft could improve forces using more prominent cases, but with a drag consequence, which enables us to make future considerations for aggressive maneuvers.

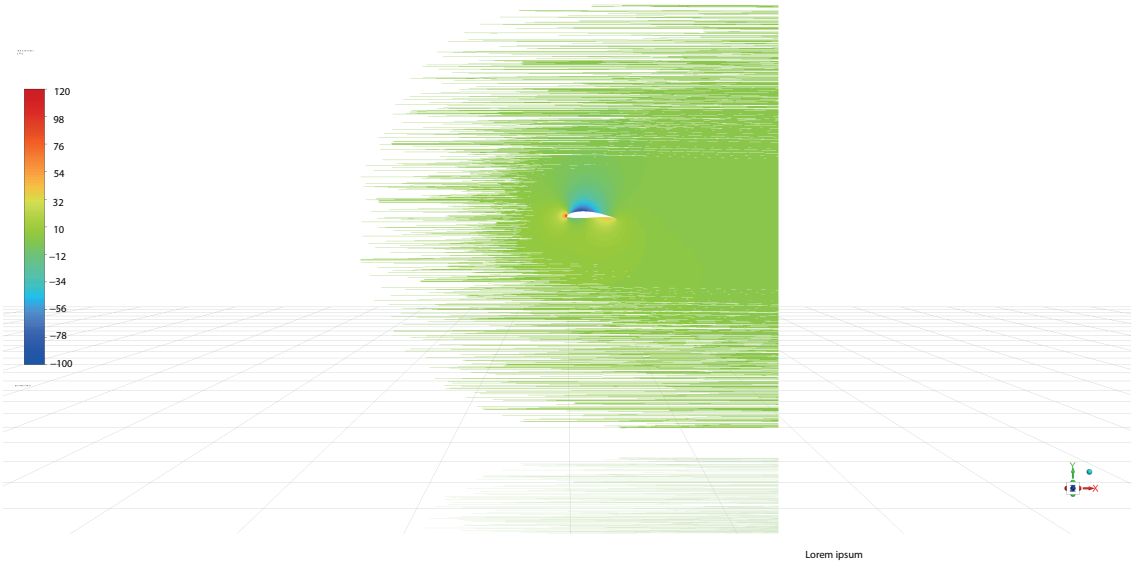


Figure 12. Pressure distribution at cruise flight.

Table 3. CFD results.

Design Point	Angle of Attack	Airspeed (m/s)	Lift (N)	Drag (N)
DP 0	0	10	1.4831801	0.18688435
DP 1	0	5	0.33591906	0.049558448
DP 2	0	14	3.0199035	0.35773087
DP 3	0	20	6.3607885	0.71587954
DP 4	1	10	1.7161523	0.21013449
DP 5	2	10	1.9474965	0.23701694
DP 6	3	10	2.1824285	0.26784294
DP 7	10	10	3.8275471	0.59171158
DP 8	15	10	4.9289569	0.9282643
DP 9	3	14	4.3934829	0.52030514
DP 10	20	14	8.181392	2.3159387
DP 11	30	14	8.2654707	4.2134698
DP 12	45	14	7.5462137	7.0732765
DP 13	−10	14	−1.1898977	0.73946404

2.3. UAV Actuation

With rapid technological advancements, integrating complex actuation systems has revolutionized the efficacy and versatility of unmanned aerial vehicles (UAVs) across various mission profiles. One of the main advantages of UAV actuation lies in its ability to augment mission adaptability and responsiveness [31]. By incorporating dynamic actuation mechanisms, such as articulated wings, tilting rotors, or swiveling thrusters, UAVs can swiftly adapt to diverse environmental conditions and operational requirements. This agility enables UAVs to navigate challenging terrains, circumvent obstacles, and execute precision maneuvers with unparalleled efficiency.

The core of our convertible UAV design lies the innovative configuration of frontal rotors featuring tilting capabilities. These rotors are actuated by precision servomotors, enabling dynamic adjustments to their orientation. This pivotal feature facilitates the seamless transition between vertical take-off and landing (VTOL) operations and cruise flight, enhancing the versatility of the UAV.

For our prototype, a tilting mechanism based on the gear transmission of the servomotor force is developed. This mechanism directly controls the tilting angle, as depicted in Figure 13. Note that the tilting rotors are independent, allowing the system to be used as a differential one. V-22 aircraft were used as inspiration for rotor placement due to their performance and wing–rotor interaction, allowing better maneuverability.

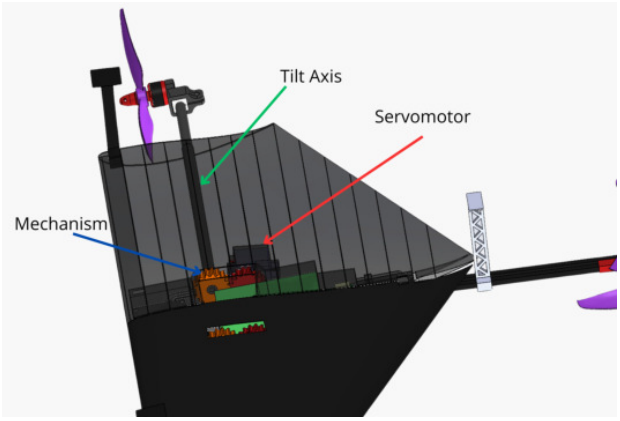


Figure 13. Tilting mechanism for rotor direction.

2.3.1. Hover Flight

Vertical Take-Off and Landing (VTOL) operations are crucial for unmanned aerial vehicles (UAVs), especially in scenarios where confined spaces or quick deployment are imperative. For our proposed vehicle in hover mode, the frontal rotors are strategically positioned vertically to generate the necessary lift and directional control, facilitating stable take-off, landing, and low-speed flight maneuvers. These rotors have precision movement capabilities, enabling orientation adjustments through tilting actions without the need for rotor speed variation. This innovative approach ensures efficiency and establishes a robust motion for hover mode control.

Furthermore, the differential control system governing the frontal rotors amplifies the CUAV agility and precision across both hover and cruise flight phases. By independently adjusting the tilt angles of each rotor, the CUAV gains precise control over pitch and yaw, facilitating seamless transitions between flight modes and empowering the vehicle to execute complex maneuvers with ease. This level of control versatility enhances operational fluidity and renders the CUAV adaptable to diverse mission requirements and environmental conditions. This condition stipulates that only saturated angles are applied to small motion, primarily utilizing the tilting mechanism for yaw motion while ensuring stability. The roll motion is obtained by the differential velocity of rotor 1 and rotor 2, and the pitch motion is obtained through the differential coupled rotors 1–2 and the coaxial rotors 3 and 4. The yaw motion is achieved by differential tilting rotors for 1 and 2; see Figure 14.

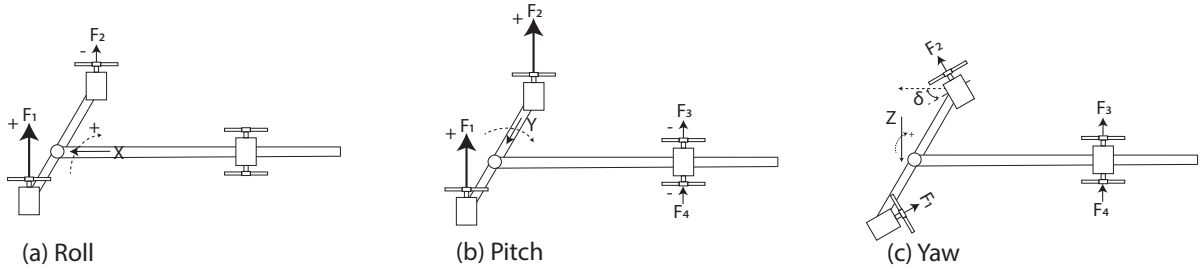


Figure 14. Diagram of tilting mechanism at low speed flight.

2.3.2. Cruise Flight

Once the UAV is airborne and ready to transition to cruise flight, the servomotors engage, facilitating the seamless transition of the rotors from vertical to horizontal orientation.

This pivotal moment marks the shift in operational dynamics as the UAV transitions from hover to fixed-wing mode. Unlike traditional aircraft configurations, where control surfaces such as ailerons, elevators, and rudders govern maneuverability, this CUAV employs a unique motion for the frontal tilting rotors.

This innovative approach highlights the control system and enhances maneuverability and responsiveness during flight. The rotor motions are defined in Figure 15, which enables responsiveness due to the strategy points used to perform an angle change of wing. By eschewing traditional control surfaces, the UAV achieves unprecedented agility and precision, enabling it to execute swift and intricate maneuvers with remarkable ease. The absence of control surfaces eliminates the associated mechanical complexities and aerodynamic constraints, allowing the UAV to push the boundaries of aerial maneuverability and operational performance.

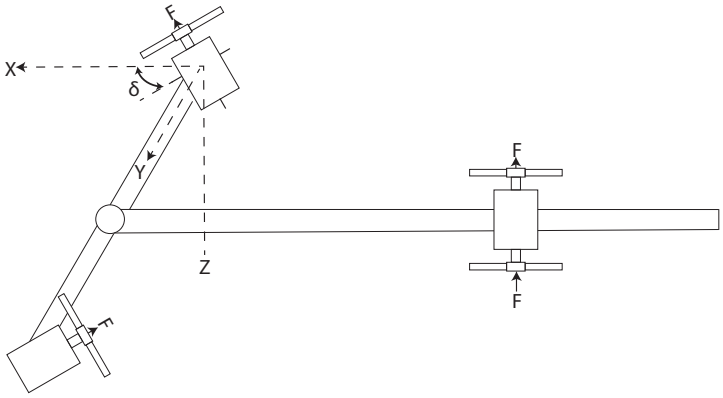


Figure 15. Tilting mechanism frame.

Furthermore, using a dual-mode capability, combining VTOL and fixed-wing flight, maximizes mission efficiency and versatility. During VTOL operations, the frontal rotors provide lift and control for take-offs, landings, and low-speed flight, ensuring operational flexibility in confined or challenging environments. Conversely, in cruise flight mode, the transition to horizontal rotor orientation optimizes aerodynamic efficiency, leveraging the fixed-wing configuration for sustained flight and extended mission endurance; see Figure 16.

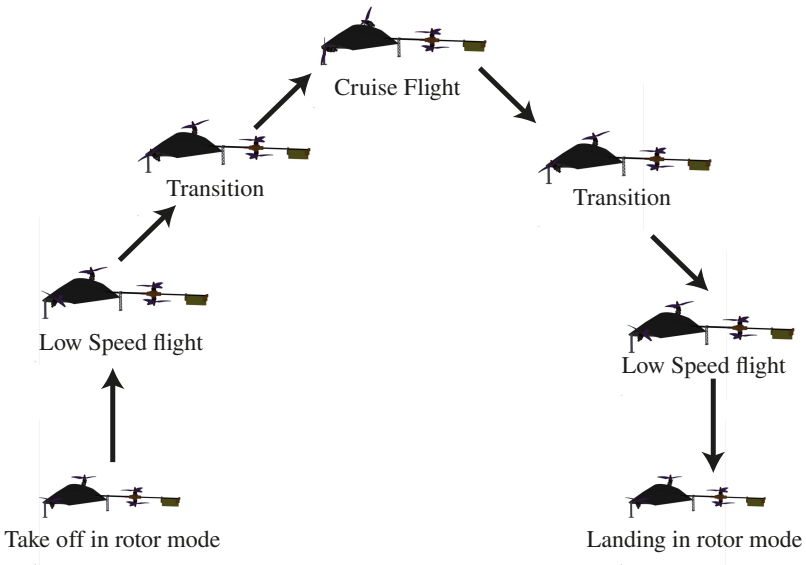


Figure 16. Hybrid mission.

2.4. Manufacturing

This innovative convertible UAV boasts a lightweight wing crafted using additive manufacturing, featuring a cutting-edge technique known as 3D printing. This method allows for the incorporation of multiple materials within the wing structure. By strategically integrating these materials, the engineers achieved an incredibly light weight without sacrificing strength. However, the benefits of additive manufacturing extend beyond the wing itself. This technology also facilitated the creation of a lattice structure within the wing. Lattice structures, resembling a complex web, offer exceptional strength-to-weight ratios, further contributing to the overall lightness of the UAV.

This lightweight design does not come at the expense of functionality. Thanks to additive manufacturing, the entire mechanism and avionics are seamlessly integrated within the interior of the wing. This ingenious approach frees up space and further streamlines the overall design of the convertible UAV.

The structural studies presented in Figures 6 and 8 aim to address the SIMP by strategically distributing bars along the wing to manage the forces. These studies were influenced by additive manufacturing techniques, specifically the interaction between walls and infill. However, in this case, these techniques served merely as inspiration. The structural points were determined based on the pressure distribution required at each point and a simplification of the SIMP algorithm, which only placed for this case a pressure point, filled by mechanical bars for this case. It was strategically distributed and filled with double the nozzle size to ensure a rigid structure.

As seen in Figure 17, this prototype utilized an improved and simplified structure that handles the forces as shown in Figure 6 and achieves maximum lightness.

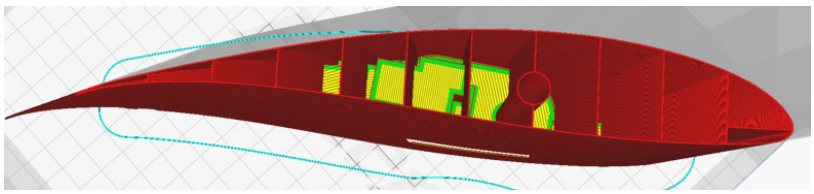


Figure 17. Internal 3D-printed wing structure.

Optimization and the use of multiple materials were key factors in the creation of the wing, as depicted in Figure 18. Several techniques were tested, but ultimately, a lattice polymeric structure, as seen in Figure 17, was chosen. Different patterns and materials exhibit different behaviors, but for this application, load distribution, as previously mentioned in Figures 6 and 8, guided the selection of the final approach.

In the realm of 3D printing, selecting the appropriate material is crucial for ensuring the quality and durability of the final product. After careful consideration, we chose ABS (acrylonitrile butadiene styrene) over PLA (polylactic acid), PETG (polyethylene terephthalate glycol), and other commonly used materials. This decision is based on the superior material stiffness and thermal deformation characteristics of ABS.

ABS is renowned for its excellent mechanical properties, particularly its high stiffness. This makes it an ideal choice for applications requiring durable and robust components. One of the significant advantages of ABS is its ability to withstand higher temperatures without deforming. ABS has a glass transition temperature of approximately 105 °C, which is significantly higher than PLA's 60 °C and PETG's 80 °C. This high thermal resistance ensures that ABS-printed parts maintain their shape and structural integrity under heat, making them suitable for a wider range of applications. ABS typically has a tensile strength of 40–50 MPa, while PLA ranges 37–50 MPa, and PETG ranges 48–55 MPa, giving us the best performance for this application



Figure 18. Multiple techniques used for wings.

2.5. Performance

Convertible aircraft, with their ability to transition between fixed-wing and rotary-wing modes, present unique challenges in performance evaluation. Unlike conventional aircraft, their performance is influenced by a complex interplay of factors, including airspeed, altitude, tilt angle, and payload. A comprehensive understanding of these interactions is crucial for optimizing aircraft design, operation, and mission planning.

The VN diagram, a fundamental tool in aerospace engineering, plays a crucial role in the design and operational planning of convertible UAVs. The VN diagram visually represents the relationship between an aircraft speed (V) and the load factor (N), providing engineers with critical insights into the aircraft's flight envelope. This diagram serves as a blueprint for understanding permissible operating limits across different flight modes for convertible UAVs.

This diagram provides a clear visualization of the operational limits of the airfoil under different load factors and velocities, as represented in Figure 19. The VN diagram analysis of our aircraft design demonstrates a well-defined range of operation, ensuring both safety and performance during various flight conditions. The evaluation indicates that the aircraft operates effectively within a speed range of 10 to 25 m per second (m/s), allowing for a versatile flight envelope.

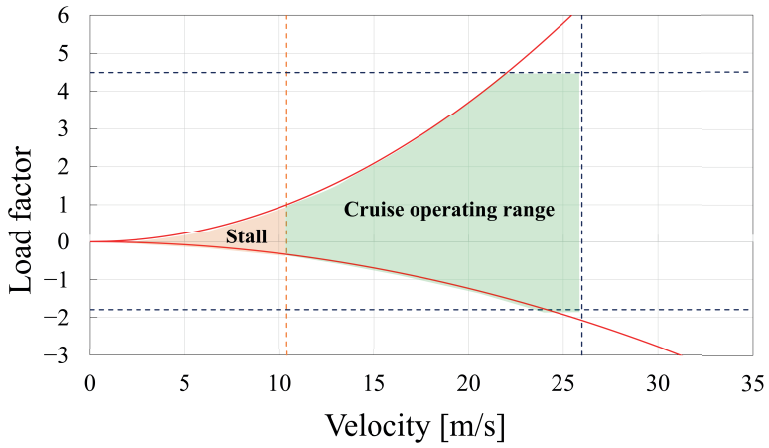


Figure 19. Flight envelope.

The stall speed of the aircraft (V_s) at $1G$, or level flight, is calculated to be approximately 10 m/s. This speed marks the minimum velocity at which the aircraft can sustain level flight without stalling. On the other end, the maximum structural speed (V_{max}) is determined to be 25 m/s. Beyond this speed, there is a risk of structural damage, and the aircraft should not be operated at these velocities.

The positive load factor limit of the aircraft is evaluated to be $+4.4G$, while the negative load factor limit is $-1.76G$. These load factor limits indicate the maximum G-forces the aircraft can safely withstand during positive and negative maneuvers. The stall speed increases at higher load factors, such as during sharp turns or sudden climbs. For instance, at a $2G$ load factor, the stall speed increases to approximately 15.6 m/s, ensuring the aircraft remains stable and controllable even during aggressive maneuvers.

The VN diagram assessment confirms that the aircraft design provides a robust operational range from 10 to 25 m/s. This range not only supports stable and efficient cruise conditions but also accommodates various maneuvering needs, including steep turns and climbs, without compromising safety. For a convertible UAV with tilting rotors, the performance surface showcases how the available payload varies with different velocities and rotor tilt angles; see Figure 20.

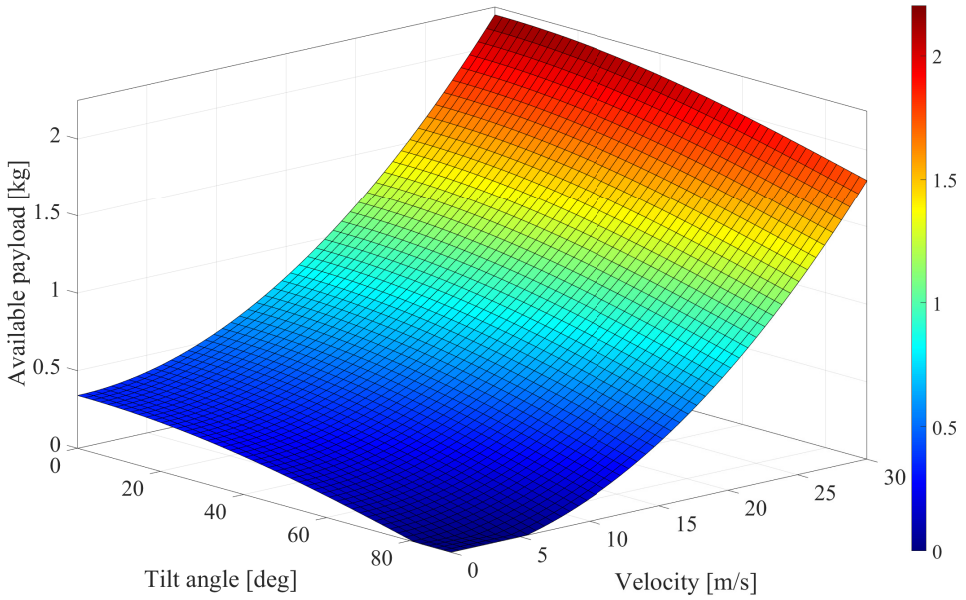


Figure 20. Performance surface for variation of the payload for each state.

The UAV is most efficient in forward flight, offering the highest payload capacity. This analysis optimizes the UAV operation for different missions, ensuring maximum payload capability while maintaining safe and efficient flight characteristics. The maximum payload is determined by the maximum hover take-off, limited by rotor forces, restricting the aircraft to 1.1 kg if the payload is at the center of mass for balanced force distribution. Figure 20 shows the system performance in each phase.

In hover mode with rotors fully tilted (0°), the UAV consumes more power, limiting the available payload to 0.4 kg. The UAV achieves better efficiency at a 45° rotor tilt and 20 m/s speed, allowing for a slightly higher available payload of 0.8 kg. The UAV reaches optimal efficiency in forward flight mode with rotors at 90° tilt, providing the highest available payload of 0.6 kg at 14 m/s.

3. Modeling and Stabilization

In this section, the equations of motion that govern the dynamic behaviors of CUAV are described. The mathematical framework, Newton–Euler equations, are used to model system dynamics, acknowledging the simplifications and assumptions inherent in these models.

The choice of reference frames is crucial in defining the 3D motion of the vehicle relative to its environment. The North–East–Down (NED) convention is considered, which is widely employed in aerospace applications, and the axes system involves the special Euclidean group SE(3). By examining the properties of SE(3) and its implications for reference frame transformations, the algorithm of guidance, navigation, and control is proposed. Note that those three reference frames are established to obtain the mathematical model of the aerial vehicles; see Figure 21.

For the vehicle orientation, Euler angles are defined as follows: ϕ is an angle defined between the x_B axis and a resultant plane from y_I and z_I; θ is an angle defined between the y_B axis and a resultant plane from x_I and z_I, and ψ is an angle defined between the z_B axis and a resultant plane from x_I and y_I. Those definitions allow aircraft to obtain attitude

stabilization in a 3D space. In this sense, two angles that provide the information in the aerodynamic or wind frame are the angle of attack α and the sideslip angle β.

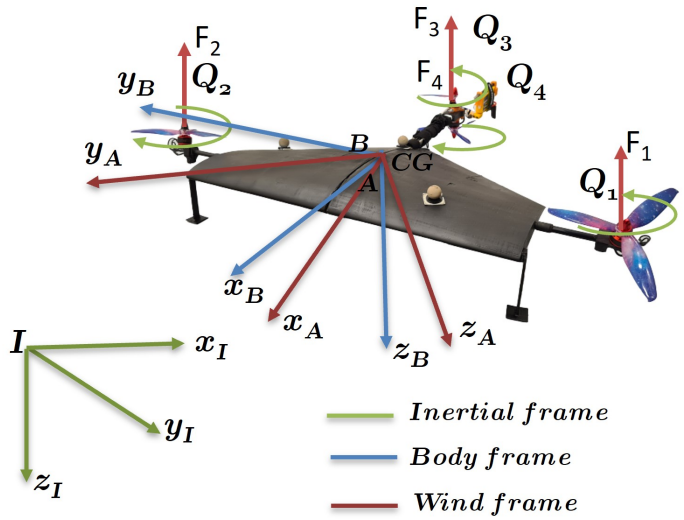


Figure 21. References frames of the CUAV.

For the tilting rotor system of proposed aircraft, an auxiliary tilting frame or rotating frame is defined about y_R, with x_{R_1}, z_{R_1}, x_{R_2}, and z_{R_2} as the principal axes, with tilting angles δ_{R_1} and δ_{R_2} as shown in Figure 22. The upwards position is 0°, while the forward position is $-\frac{\pi}{2}$°according to the NED (North–East–Down) convention and the right-hand rule.

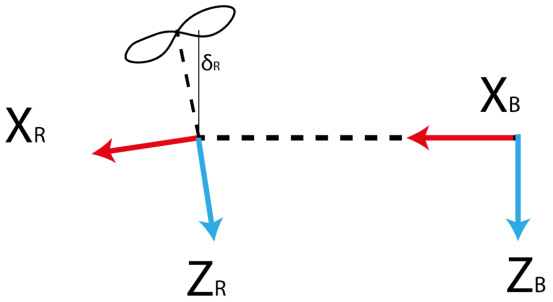


Figure 22. References frame for angular rotation.

3.1. Equations of Motion

The model of the vehicle considers an inertial fixed frame as $\mathcal{I} = \{x_\mathcal{I}, y_\mathcal{I}, z_\mathcal{I}\}$ and a body frame fixed attached to the center of gravity of the vehicle as $\mathcal{B} = \{x_\mathcal{B}, y_\mathcal{B}, z_\mathcal{B}\}$. The wind frame $\mathcal{A} = \{x_\mathcal{A}, y_\mathcal{A}, z_\mathcal{A}\}$ is considered during the forward flight [32] (see Figure 23). The configuration of the convertible UAV is defined by the location of the center of gravity and the attitude with respect to the inertial frame. Then, the configuration manifold is the special Euclidean group SE(3), which is the semidirect product of $\mathbb{R}^3$ and the special orthogonal group SO(3).

The Newton–Euler formulation, for a rigid body, is used in order to obtain the mathematical model as

$$\dot{\xi} = V \tag{1}$$

$$m\dot{V} = RF + mge_3 + D_\xi(t) \tag{2}$$

$$\dot{R} = R\hat{\Omega} \tag{3}$$

$$J\dot{\Omega} = -\Omega \times J\Omega + \tau_a + D_\eta(t) \tag{4}$$

where $\xi = (x, y, z)^\top \in \mathbb{R}^3$ and $V = (v_x, v_y, v_z)^\top \in \mathbb{R}^3$ are the position coordinates and translational velocity relative to the inertial frame. $\eta = (\phi, \theta, \psi)^\top \in \mathbb{R}^3$ describes the rotation coordinates where ϕ, θ, and ψ represent the roll, pitch, and yaw or heading, respectively. e_1, e_2, and e_3 are the vectors of the canonical basis of $\mathbb{R}^3$ in $\mathcal{I}$. The rotation matrix, $R \in \mathrm{SO}(3) : \mathcal{B} \to \mathcal{I}$, satisfies the $\mathrm{SO}(3) = \left\{R \mid R \in \mathbb{R}^{3\times3}, \det[R] = 1, RR^\top = R^\top R = I\right\}$ and is parameterized by the Euler angles ϕ, θ, and ψ. The rotation matrix is written as

$$R = \begin{pmatrix} c_\theta c_\psi & s_\phi s_\theta c_\psi - c_\phi s_\psi & c_\phi s_\theta c_\psi + s_\phi s_\psi \\ c_\theta s_\psi & s_\phi s_\theta s_\psi + c_\phi c_\psi & c_\phi s_\theta s_\psi - s_\phi c_\psi \\ -s_\theta & s_\phi c_\theta & c_\phi c_\theta \end{pmatrix}$$

where the shorthand notation of $s_a = \sin(a)$ and $c_a = \cos(a)$ is used. $\Omega = (p, q, r)^\top \in \mathbb{R}^3$ is the angular velocity in $\mathcal{B}$, where the heat map $\hat{}: \mathbb{R}^3 \to \mathfrak{so}(3)$ is defined by the condition that $\hat{a}b = a \times b$ for all $a, b \in \mathbb{R}^3$.

$$\hat{\Omega} = \begin{pmatrix} 0 & -r & q + \dot{\delta_{R_1}} \\ r & 0 & -p - \dot{\delta_{R_2}} \\ -q - \dot{\delta_{R_1}} & p + \dot{\delta_{R_2}} & 0 \end{pmatrix} \tag{5}$$

where δ_{R_1} and δ_{R_1} are the tilting angles.

The forces acting on the body frame are described as follows:

$$F = \begin{bmatrix} F_{x_B} \\ F_{y_B} \\ F_{z_B} \end{bmatrix} = \begin{bmatrix} 0 \\ 0 \\ -F_3 \end{bmatrix} + \begin{bmatrix} 0 \\ 0 \\ -F_4 \end{bmatrix} + \begin{bmatrix} -F_1 \sin(\delta_{R_1}) \\ 0 \\ -F_1 \cos(\delta_{R_1}) \end{bmatrix} + \begin{bmatrix} -F_2 \sin(\delta_{R_2}) \\ 0 \\ -F_2 \cos(\delta_{R_2}) \end{bmatrix} \tag{6}$$

where $F = (F_{x_B}, F_{y_B}, F_{z_B})^\top \in \mathbb{R}^3$ is the vector of the total forces in the x, y, and z axes, respectively. F_i is the lift force or thrust force of the propeller for $i = 1, 2, 3, 4$.

In hover mode ($\delta_{R_1} = 0$ and $\delta_{R_2} = 0$), (6) becomes

$$F = \begin{bmatrix} F_{x_B} \\ F_{y_B} \\ F_{z_B} \end{bmatrix} = \begin{pmatrix} 0 \\ 0 \\ -(F_1 + F_2 + F_3 + F_4) \end{pmatrix} \tag{7}$$

In cruise mode ($\delta_{R_1} \approx \frac{\pi}{2}$ and $\delta_{R_2} \approx \frac{\pi}{2}$), (6) becomes

$$F = \begin{bmatrix} F_{x_B} \\ F_{y_B} \\ F_{z_B} \end{bmatrix} = \begin{pmatrix} -(F_1 + F_2) \\ 0 \\ -(F_3 + F_4) \end{pmatrix} \tag{8}$$

For external forces, we include specially aerodynamics ones, defining them as

$$D_\xi = \begin{pmatrix} d_{\xi_1} \\ d_{\xi_2} \\ d_{\xi_3} \end{pmatrix} = RW^T \begin{pmatrix} D_a \\ Y_a \\ L_a \end{pmatrix} \tag{9}$$

where the rotation aerodynamic matrix $W : \mathcal{B} \to \mathcal{A}$ that transforms a force from the body frame to the aerodynamic frame is described as

$$W = \begin{pmatrix} c_\alpha c_\beta & s_\beta & s_\alpha c_\beta \\ -c_\alpha s_\beta & c_\beta & -s_\alpha s_\beta \\ -s_\alpha & 0 & c_\alpha \end{pmatrix}$$

where α is the angle of attack and β is the sideslip angle. L, Y, and D are the aerodynamic forces: lift, side force, and drag, respectively [32].

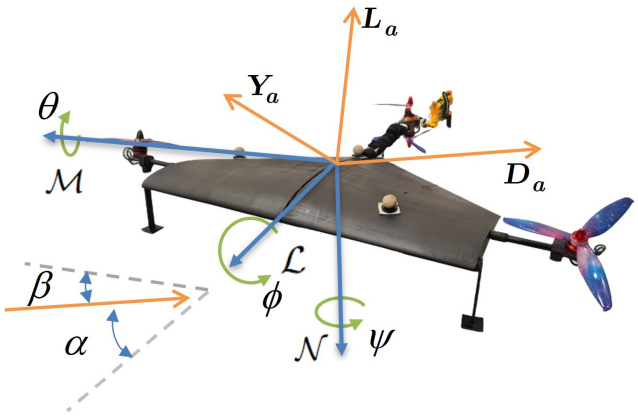


Figure 23. Aerodynamic forces of the CUAV.

In the context of torque analysis within the aircraft dynamics, the torque vector τ_a is defined at the center of gravity with a pivotal point corresponding to the body frame. This representation provides the rotational dynamics of the aircraft and is derived from the collective effects of the four-rotor forces. This torque is formulated as follows:

$$\tau_a = \begin{pmatrix} \tau_\phi \\ \tau_\theta \\ \tau_\psi \end{pmatrix} = \begin{pmatrix} d(F_1 - F_2) \\ l_2(F_3 + F_4) - l_1(F_1 + F_2) + \tau_{wing} \\ Q_1 + Q_3 - Q_2 - Q_4 + F_1 \sin(\delta_{R_1}) - F_2 \sin(\delta_{R_2}) \end{pmatrix} \tag{10}$$

where $\tau_{wing} = C_{m,wing} \frac{1}{2} \rho V^2 S_{wing} c_{wing} \Delta\alpha$ encompasses the contributions stemming from the frontal wing; here, $C_{m,wing}$ is the pitching moment coefficient of the wing, ρ is the air density, V is the airspeed of the aircraft, S_{wing} is the wing area, c_{wing} is the average chord length of the wing, and $\Delta\alpha$ is the change in angle of attack of the wing. $Q_i = \rho A_i r_i^3 c_{Q_i} \omega_i^2$, where A_i is the rotor disk area, r_i is the rotor radius, c_{Q_i} denotes the rotor shaft moment coefficient and ω_i denotes the angular velocity of the rotor i with $i = 1, 2, 3, 4$. d stands for arm length; l_1 and l_2 represent distances to the center of mass.

The moments acting on the aerial vehicle are described

$$D_\eta = \begin{pmatrix} d_{\eta 1} \\ d_{\eta 2} \\ d_{\eta 3} \end{pmatrix} = d_{\eta gyro} + d_{\eta aero} \tag{11}$$

The gyroscopic moment generated by the rotation of the airframe and the four rotors is described by

$$d_{\eta gyro} = \sum_{k=1}^{4} (-1)^{k+1} I_{r_k} [\Omega \times e_3 \omega_k] \tag{12}$$

Finally, the aerodynamic moments presented on the airframe are described as

$$d_{\eta aero} = \begin{pmatrix} \mathcal{L} & \mathcal{M} & \mathcal{N} \end{pmatrix}^\top$$

where $\mathcal{L}$, $\mathcal{M}$ and $\mathcal{N}$ are the aerodynamic rolling, pitching and yawing moments, respectively [5,32].

Using Equations (1)–(4), a nonlinear set of equations can be described as

$$\begin{array}{rcl}
\dot{x} & = & v_x \\
\dot{y} & = & v_y \\
\dot{z} & = & v_z \\
\dot{v}_x & = & \frac{F_{x_B}}{m}\left(c_\theta c_\psi\right) + \frac{F_{y_B}}{m}\left(s_\phi s_\theta c_\psi - c_\phi s_\psi\right) + \frac{F_{z_B}}{m}\left(c_\phi s_\theta c_\psi + s_\phi s_\psi\right) + d_{\xi_1} \\
\dot{v}_y & = & \frac{F_{x_B}}{m}\left(c_\theta s_\psi\right) + \frac{F_{y_B}}{m}\left(s_\phi s_\theta s_\psi + c_\phi c_\psi\right) + \frac{F_{z_B}}{m}\left(c_\phi s_\theta s_\psi - s_\phi c_\psi\right) + d_{\xi_2} \\
\dot{v}_z & = & \frac{F_{x_B}}{m}\left(-s_\theta\right) + \frac{F_{y_B}}{m}\left(s_\phi c_\theta\right) + \frac{F_{z_B}}{m}\left(c_\phi c_\theta\right) + g + d_{\xi_3} \\
\dot{\phi} & = & p + q\sin(\phi)\tan(\theta) + r\cos(\phi)\tan(\theta) \\
\dot{\theta} & = & q\cos(\phi) - r\sin(\phi) \\
\dot{\psi} & = & q\sec(\theta)\sin(\phi) + r\sec(\theta)\cos(\phi) \\
\dot{p} & = & \left(\frac{J_{yy}-J_{zz}}{J_{xx}}\right)qr + \left(\frac{1}{J_{xx}}\right)\tau_\phi + d_{\eta 1} \\
\dot{q} & = & \left(\frac{J_{zz}-J_{xx}}{J_{yy}}\right)pr + \left(\frac{1}{J_{yy}}\right)\tau_\theta + d_{\eta 2} \\
\dot{r} & = & \left(\frac{J_{xx}-J_{yy}}{J_{zz}}\right)pq + \left(\frac{1}{J_{zz}}\right)\tau_\psi + d_{\eta 3}
\end{array} \tag{13}$$

Remark 1. *As the rotation of the four propellers on the convertible UAV is balanced, the gyroscopic moment will essentially be zero. The only cases in which gyroscopic moments will not be zero are if there is a significant difference in the RPM of the four motors and the presence of a strong sideways cross-wind.*

Remark 2. *The design of the convertible UAV is based on in a configuration that optimizes the aerodynamic properties and reduces drag forces, which provides steady flights. In addition, the wing involves a damping that reduces the transient or oscillatory motion, specifically unstable spiral roll.*

Based on the remarks, the disturbance terms D_η and D_ξ satisfy the linear growth bound as $\| D_\xi \| \leq c_\xi \ \forall t$ and $\| D_\eta \| \leq c_\eta \ \forall t$.

3.2. Guidance, Navigation and Control Algorithm

The guidance, navigation, and control of the convertible UAV is based on a geometric tracking control in SE(3) (special Euclidean group); see [33]. The control is a saturated proportional, integral, and derivative (PID) and provides smooth trajectory tracking based on SE(3) even in the presence of wind disturbances. For this purpose, the Equation (13) can be rewritten as

For this purpose, Equation (13) can be rewritten as

$$\dot{\xi} = V \tag{14}$$

$$\dot{V} = u_n + d_\xi(t) \tag{15}$$

$$\dot{R} = R\hat{\Omega} \tag{16}$$

$$\dot{\Omega} = u_a + d_R(t) \tag{17}$$

where $u_n \in \mathbb{R}^3$ and $u_a \in \mathbb{R}^3$ are virtual control inputs for the position and orientation dynamics. $d_\xi(t) = \frac{D_\xi(t)}{m}$ and $d_R(t) = J^{-1}[-\Omega \times J\Omega + D_\eta(t)]$.

For a smooth transition, a condition is defined in order to ensure that at each instant of time, at most one of the two control inputs is active. The geometric navigation considers a guidance frame that is designed to perform autonomous flights with a convergence to the contour of the task with small normal velocity.

$$u_n = u_{n_1} g_1(t) + u_{n_2} f_1(t) \tag{18}$$

$$f_1(t) = \begin{cases} 0 & for \quad 0 \leq t < T_1 \\ 1 & for \quad T_1 \leq t \leq T_F \end{cases} \text{ with } g_1(t) = 1 - f_1(t) \tag{19}$$

For hover flight, $0 \leq t < T_1$, the virtual control input u_{n_1} is defined as

$$u_{n_1} = ge_3 - \frac{RF}{m} \tag{20}$$

For cruise mode, $T_1 \leq t \leq T_F$, the virtual control input u_{n_2} is defined as

$$u_{n_2} = ge_3 - \frac{RF}{m} \tag{21}$$

For orientation dynamics, the virtual control input u_a is defined as

$$u_a = J^{-1}\tau_a \tag{22}$$

Remark 3. *The transition maneuver of the CUAV, from hover to cruise modes and vice versa, is smooth, and it starts when the vehicle reaches the hovering flight in the initial or actual waypoint, i.e., $F_{z_B} \approx mg$; after that, the transition starts, and the cruise mode is performed until the CUAV arrives to the final waypoint to return to the hovering flight.*

Definition 1. *A guidance frame $\mathcal{G}=\{f_g, b_g, n_g\}$ is a reference frame that consists of the control forward vector f_g, the control binormal vector b_g and the control normal vector n_g. This frame satisfies the NED (North–East–Down) system and considers the terminology from the names of the three unit vectors in the reference frame for a curve in $\mathbb{R}^3$.*

The three vectors are defined as follows (for more details, see [33]):

- The control normal vector n_g is defined as a function of the position and velocity errors.

$$n_g = \frac{ge_3 - u_n}{\|ge_3 - u_n\|} \tag{23}$$

- The control forward vector f_g is defined as a unit vector in the (n_g, t_d) plane and is orthogonal to n_g such as $n_g \cdot t_d > 0$ with $t_d = \frac{\dot{\xi}_d}{\|\dot{\xi}_d\|}$. Then

$$f_g = \frac{n_g \times e_1}{\|n_g \times e_1\|} \tag{24}$$

- The control binormal vector b_g is defined as

$$b_g = -(f_g \times n_g) \tag{25}$$

Definition 2. *A desired rotation matrix $R_d \in SO(3)$ is defined as $R_d = [f_g \;\; b_g \;\; n_g]$ corresponding to the reference frame or guidance frame where $f_g = R_d e_1$, $b_g = R_d e_2$ and $n_g = R_d e_3$.*

From [33], the next statements are well known.

1. $u_n \neq ge_3$;
2. n_g is a well-defined unit vector;
3. f_g is a well-defined unit vector;
4. $\{f_g \;\; b_g \;\; n_g\}$ is orthonormal and the matrix $R_d = [f_g \;\; b_g \;\; n_g]$.

Establishing a guidance frame enables the development of a control strategy that allows the introduction of u_n as an input while utilizing position references as feedback. In this case, a classical proportional, integral, and derivative (PID) control scheme is proposed. A navigation scheme using this type of control can be effective, providing accurate feedback and a sufficiently responsive system. For this purpose, the following PID saturated structure is utilized [34].

The position control for the CUAV is proposed as follows:

$$u_n = \text{Sat}\left(k_{p_{\tilde{\xi}}} e_{\tilde{\xi}} + k_{d_{\tilde{\xi}}} \dot{e}_{\tilde{\xi}} + k_{i_{\tilde{\xi}}} \int e_{\tilde{\xi}} dt \right) \tag{26}$$

where $e_{\tilde{\xi}} = \xi_d - \xi$, $\dot{e_{\tilde{\xi}}} = \dot{\xi}_d - \dot{\xi}$ are the position and velocity errors. $k_{p_{\tilde{\xi}}}$, $k_{d_{\tilde{\xi}}}$ and $k_{i_{\tilde{\xi}}}$ stand for the diagonal and positive definite matrices. The stability analysis of this saturated control can be found in [35]

A similar procedure is used to propose the control to orientation dynamics, u_a , considering the rotation desired matrix $R = [f_g \;\; b_g \;\; n_g]$, which corresponds to the reference frame. Based on the group operation of SO(3), the attitude and the angular velocity errors are defined as $R_e = RR_d^\top$ and $e_\Omega = \Omega_d - \Omega$.

The orientation control is described as

$$u_n = \text{Sat}\left(k_{p_\Omega} e_R + k_{d_\Omega} \dot{e}_\Omega + k_{i_\Omega} \int e_R dt \right) \tag{27}$$

where $e_R = \text{Skew}(\text{RR}_\text{d}^\top)^\vee$, with $\text{Skew}(\text{A}) = \frac{1}{2}(\text{A} - \text{A}^\top)$ and the operator $(\cdot)^\vee$ is the inverse of the "hat" operator. k_{p_Ω}, k_{d_Ω} and k_{i_Ω} stand for the diagonal and positive definite matrices [33].

A dual-layer controller architecture is utilized to enhance the navigation and attitude control of the convertible aircraft. This approach comprises two distinct layers. The first layer focuses on rate control, using velocity for translational motion and angular velocity for rotational motion. The second layer is dedicated to position control for translational motion and attitude control for rotational motion. By combining both layers, the system produces a final output that effectively guides the aircraft.

The dual-layer controllers follow the same structure previously mentioned but with a hierarchical arrangement. Instead of explicitly presenting the equations, the interaction between the two layers is emphasized for clarity. This arrangement ensures smooth integration and coordination between rate and position control, enabling precise and responsive navigation and attitude control for the convertible aircraft; see Figure 24.

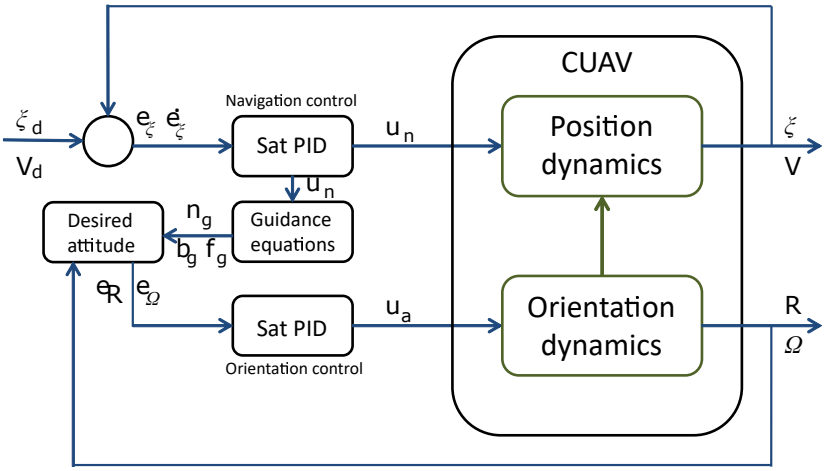


Figure 24. Guidance, navigation and control scheme for the CUAV.

4. Real-Time Validation

In order to validate the vehicle and the proposed GNC algorithm, a design of experiments (DoE) is executed in an indoor environment, performing the capabilities of the proposed system. The experiments focus on trajectory tracking tests, which facilitate the assessment of the system performance under consistent patterns and diverse movement combinations. However, specific missions are performed for convertible aircraft to evaluate the system across various scenarios.

The tests are carried out in the Navigation Laboratory at the Aerospace Engineering Research and Innovation Center of the Faculty of Mechanical and Electrical Engineering at the Autonomous University of Nuevo Leon. This laboratory features 16 VICON T-40 cameras to obtain the localization measurements; see Figure 25.

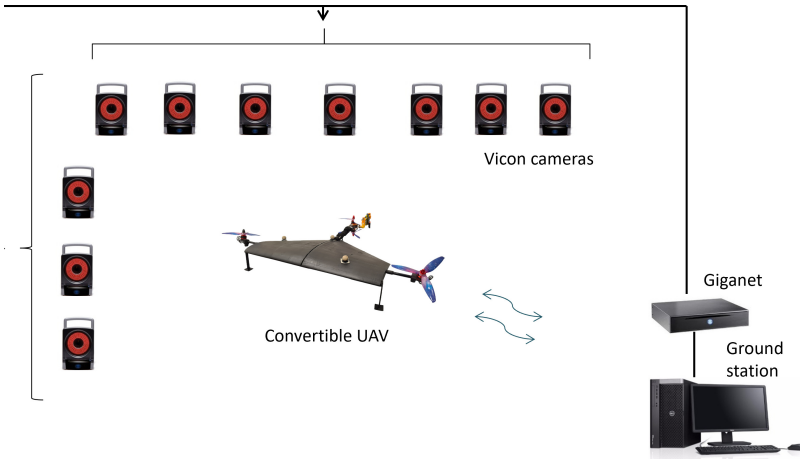


Figure 25. Tracking system.

The ground station receives and sends the information to the autopilot systems, and the interface is developed in order to graph the state variables of the system; see Figure 26.

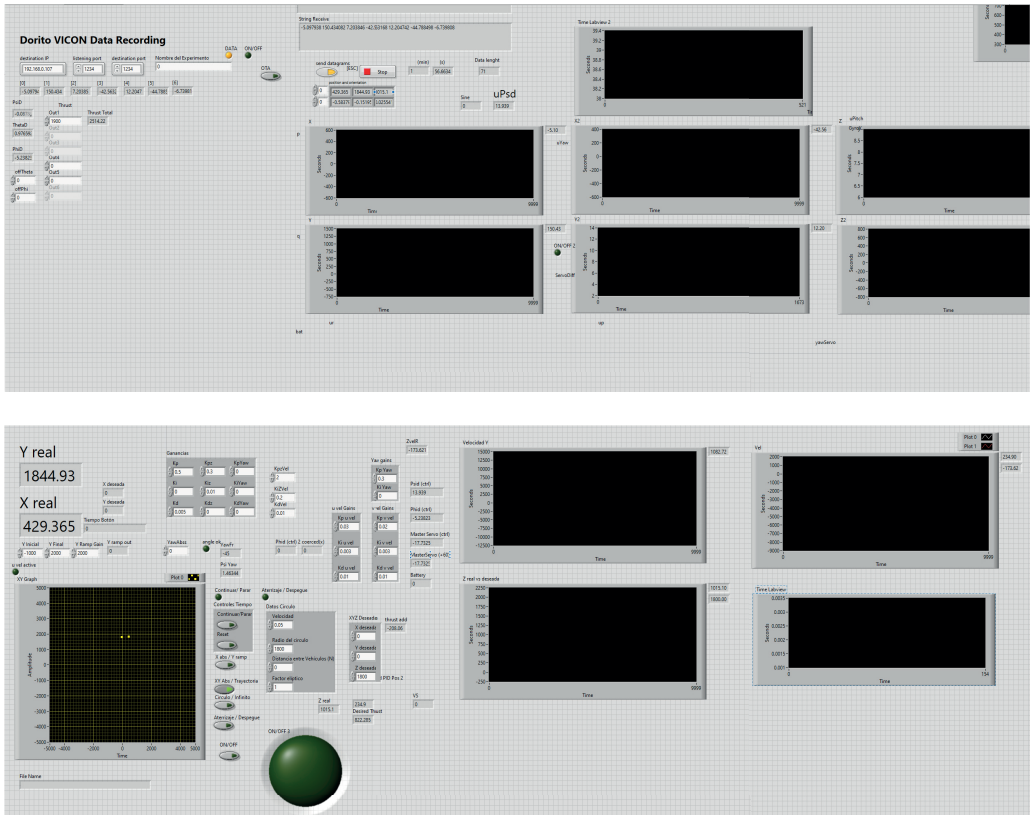


Figure 26. CUAV interface in the ground station.

The proposed CUAV is equipped with a low-cost avionics system developed by our laboratory, allowing us to access the whole state variables of the system. For the inner loop, the attitude is obtained via the estimation method, i.e., the complementary filter in SE(3), while for the outer loop, the position is obtained through estimation by the tracking system. The scheme of the aircraft is shown in Figure 27, providing a homemade autopilot in order

to manipulate the complete systems for flights in real-time. For that reason, it is possible to debug the system on each of its steps, and Figure 28 illustrates the real-time experiments.

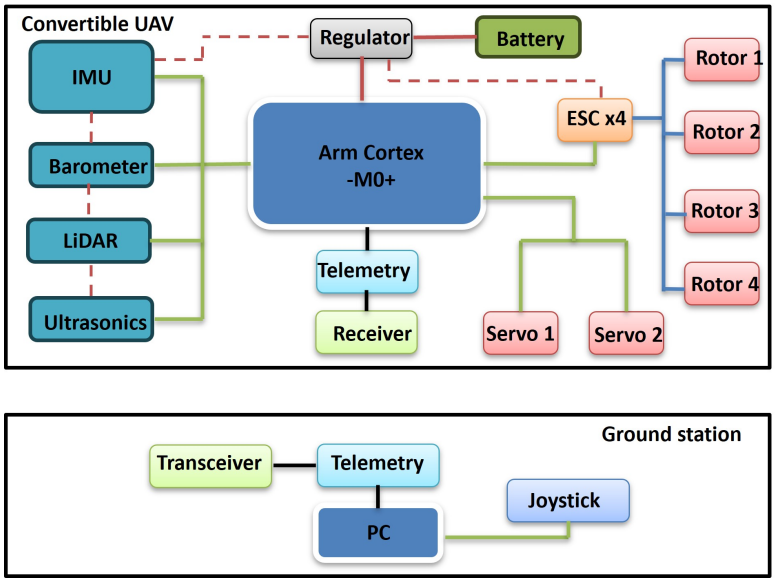


Figure 27. Flight computer scheme.

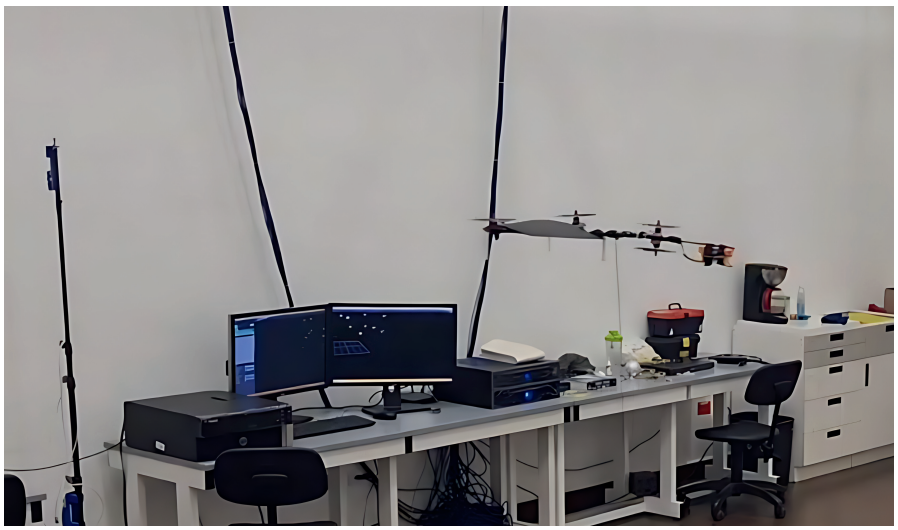


Figure 28. Real-time flight of the CUAV.

The experiments that are executed for this prototype enable the characterization of the system and the identification of unexpected behaviors. In this sense, specific paths and input ramp signals are selected for testing. Notably, these experiments are run in real-time, and the information about state variables is sent to the ground station. The camera system is essential for data tracking, requiring using a bounded environment for experimentation. Despite these constraints, the selected paths and input ramps provide valuable insights into the system performance and behavior under controlled conditions. The information is tracked during this experiment, including position data, sensor readings, and control inputs, which are recorded in a data file for analysis.

The experiments selected are those represented in Table 4.

Table 4. Design of experiments.

Experiment	Description
Circle	Circle pattern with tangent tracking, fixed Z, and multiple experiments development for dependence on velocity
Infinite	Complex pattern for whole system test; combined capabilities are tested
Tilting ramp	Tilting rotor test for control test, which required an input similar to a forward flight with a process of stopping at the end of the path
Fast line	Test for max linear velocity in controlled environment

4.1. Circle

For the circular trajectory, we selected a circle with a radius of 1750 mm, a height of 1800 mm, and a velocity of 0.03 rev/s. For this case, the tilting mechanism is assessed, which allows us to have that type of motion without using input on the rotors; those are only controlled by the mixer for stabilization purposes.

Geometrical errors, a natural consequence of the lower resolution on actuators, are a significant factor in our trajectory. These errors are visualized by a circle made of trajectories based online. Despite these challenges, the trajectory remains within correct values with some drift but an acceptable tracking error; see Figure 29.

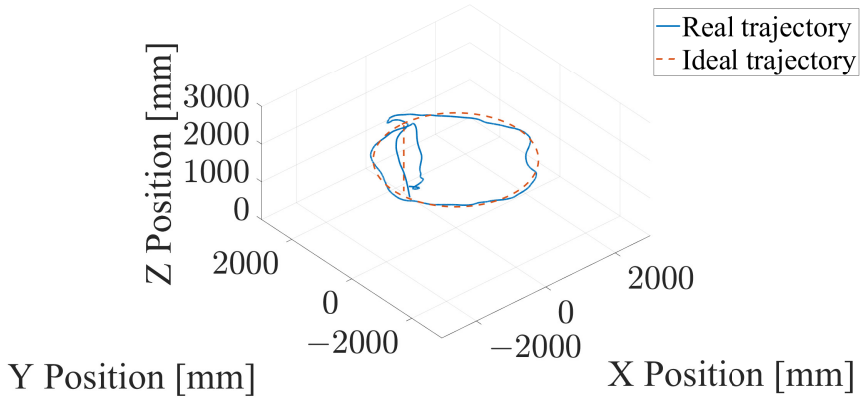


Figure 29. XYZ trajectory tracking, real vs. ideal.

One of the objectives of this design is to ensure that the pitch angle is as small as possible, especially so as not to interfere with the forces generated by the wing. As a result, it is shown that the system follows the system with 100 mm of maximum error and ±3 of angle error; see Figure 30.

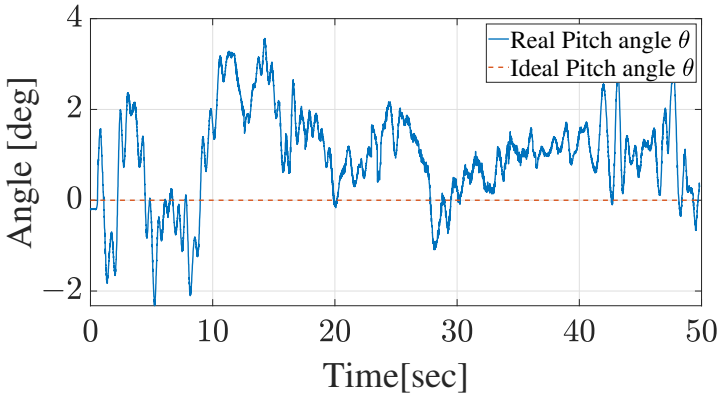


Figure 30. Pitch angle, real vs. ideal (low pitch).

4.2. Infinite

While the circular path experiment provides valuable insights into maintaining a constant radius, a separate experiment simulating an infinite straight path is equally important. This allows us to evaluate the system ability to handle long-distance navigation and drift correction, which is crucial for real-world applications like long-range surveillance. A complex trajectory is tested for an infinite trajectory, and a control signal response is illustrated; see Figure 31.

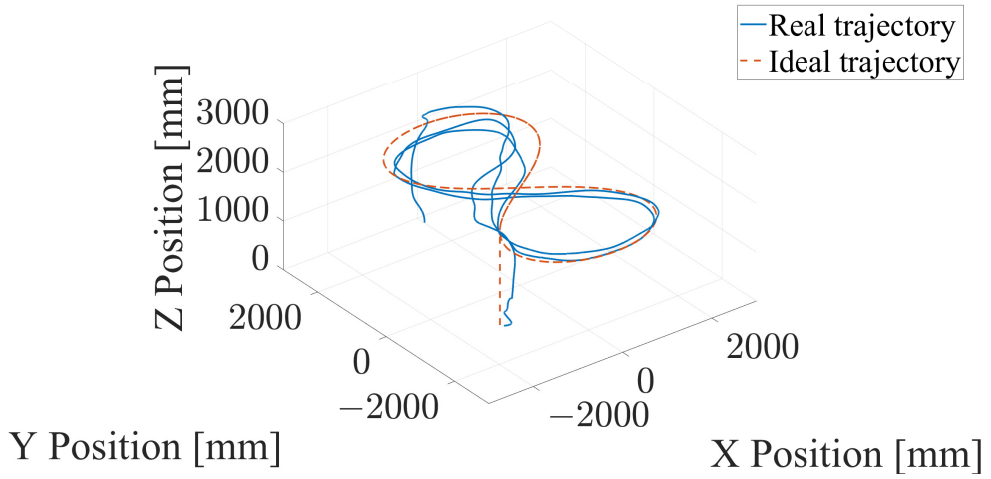


Figure 31. XYZ trajectory tracking, real vs. ideal.

As seen before, the CUAV accomplishes and follows this trajectory with a deviation of 200 mm; this behavior is expected because the system is performing a transition phase, which involves uncertainty to be solved for the proposed GNC algorithm. The form control field shows that the system is tracking signals; errors are expected from the external sensor data; see Figure 32.

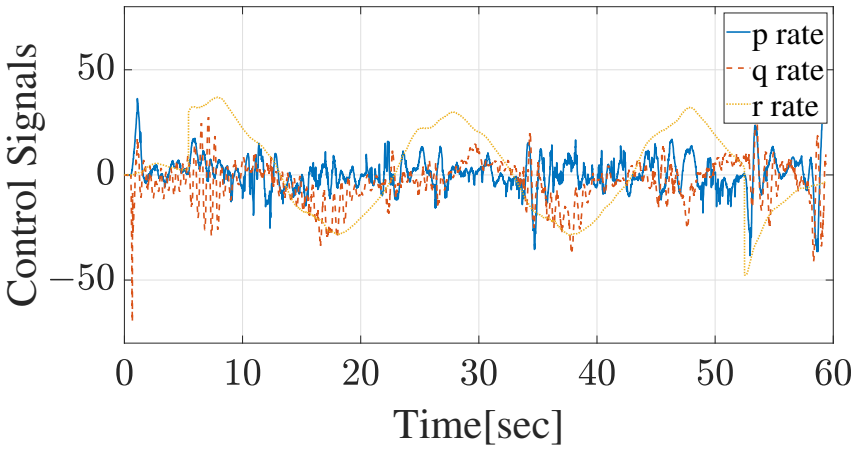


Figure 32. Control signals on infinite trajectories.

4.3. Tilting Ramp

This experiment shows the fast transition of the system on a tilting rotor, where the input is a fast change on tilting angles, as shown in Figure 33.

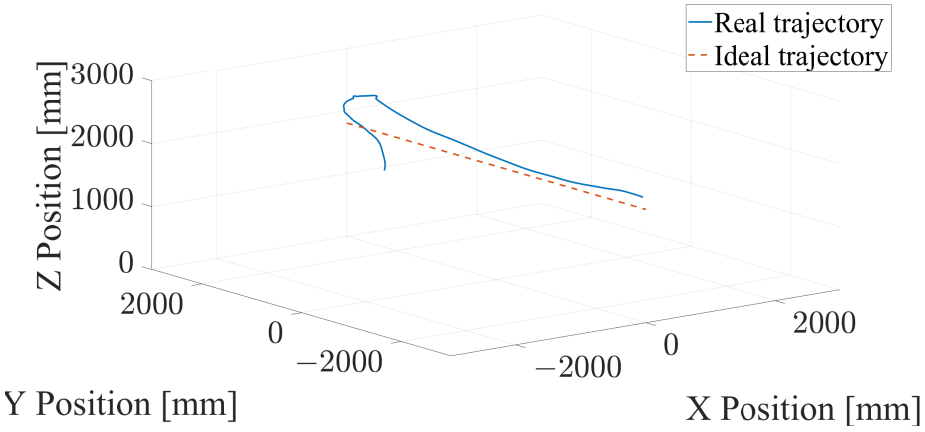


Figure 33. XYZ trajectory tracking, real vs. ideal.

For this case, a straight line is developed to change between hover and cruise flight. In this short-period experiment, the control scheme compensates for height loss. Also, it accelerates the CUAV, performing a maximum of 2 m/s, where it is realized that the system is still in hover mode, and rotors do not make the whole change. However, it is a short-period experiment showing the expected accomplishment of dynamics; see Figure 34.

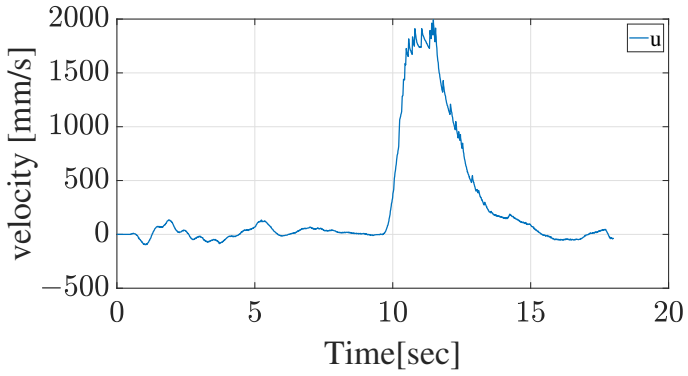


Figure 34. U velocity develop at ramp.

As seen in Figure 35, at 10 to 12 s, the system increases lift, which is directly seen as a decrease in the signal required for the system to maintain height.

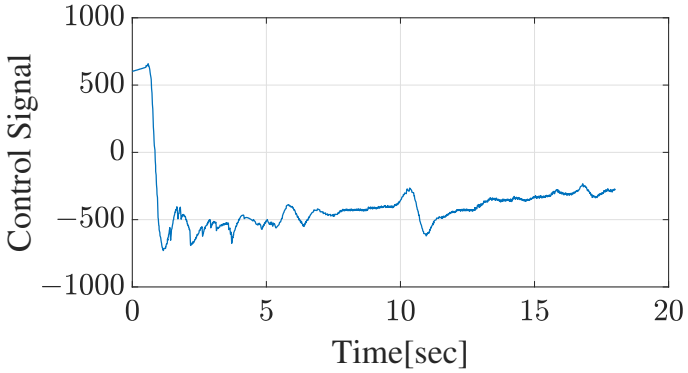


Figure 35. Lift behavior on global rotor forces.

4.4. Fast Line—Transition Mode

In this section, we present a development of an experiment where the aircraft is tested on maximum velocity conditions indoors. The line design is 5 m on the same axis, and the

initial condition is used to execute a hover flight, followed by a fast line, and end with an instant decrease of velocity on the system; see Figure 36.

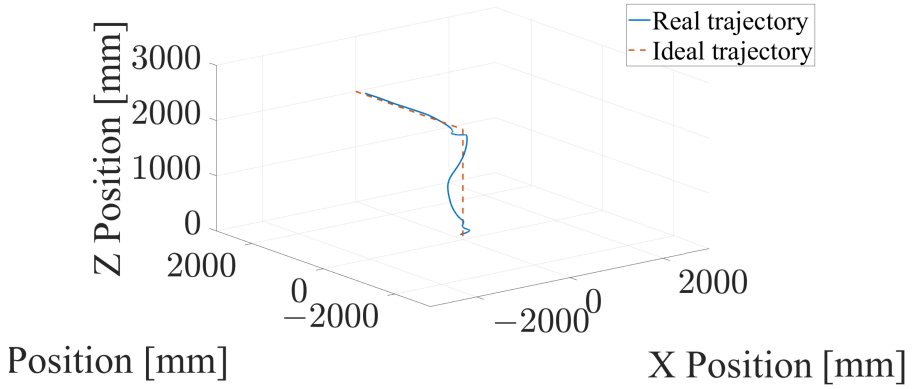


Figure 36. XYZ trajectory tracking, real vs. ideal.

The vehicle followed the trajectory even under demanding conditions. Some errors are expected, in this case, 300 mm on average; see Figure 37.

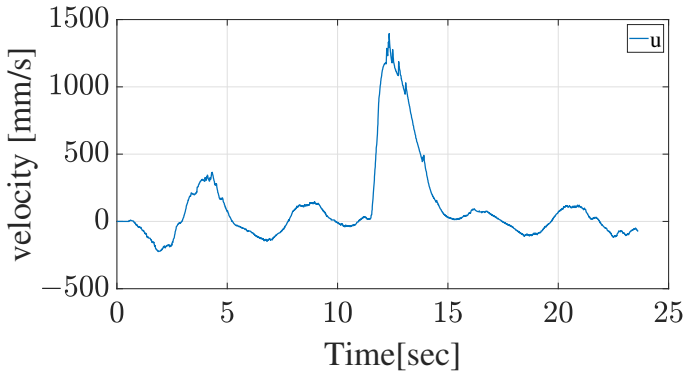


Figure 37. U velocity developed at the line.

Even the maximum condition on the system is required; just 3.7 m/s is reached due to space limitations. On a complete flight, the cruise phase is performed considering a change about 55°reached by the tilting rotors during the transition phase. In the transition phase, the vehicle reaches 90°on a complete transition, as can be seen in Figure 38.

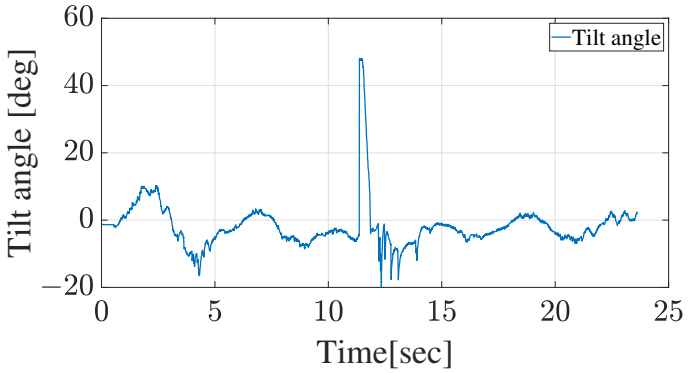


Figure 38. Servos transition phase.

In the following link, a test video is shown: https://youtu.be/h5RhDCh6QtQ?si=5VnO1xTrUZ-YuJhN accessed on 11 February 2024. It is important to mention that a circle experiment was developed in this video.

5. Conclusions

The design of a convertible UAV platform capable of executing hover and cruise flight missions was presented, having characteristics of a helicopter and an aircraft. The design was validated by taking into account the structural refinement and airfoil-based design methodology; each stage addressed critical aspects of design based on conceptual aerodynamics, mechanical properties, and material selection. Additive manufacturing was used to develop the proposed vehicle, considering the optimization techniques used to obtain a lightweight vehicle structure. The control strategy provided an effective performance for hover and cruise flights of the convertible UAV, and it was designed to ensure complete flight regimes. Notable achievements included reduced control authority reliance on rotors and effective lift generation by the main wing during cruise flights. Validation experiments, encompassing the convertible UAV approach, revealed promising results in trajectory tracking and efficient flight maneuvers.

Author Contributions: Conceptualization, E.U.R.-R.; methodology, E.U.R.-R.; software, E.U.R.-R. and E.G.R.-R.; validation, E.U.R.-R. and S.A.A.-E.; formal analysis, E.U.R.-R. and O.G.-S.; investigation, S.A.A.-E. and O.G.-S.; resources, O.G.-S.; data curation, E.G.R.-R. and S.A.A.-E.; writing—original draft preparation, E.U.R.-R.; writing—review and editing, E.U.R.-R. and S.A.A.-E.; visualization, E.G.R.-R. and S.A.A.-E.; supervision, O.G.-S.; project administration, O.G.-S.; funding acquisition, O.G.-S. All authors have read and agreed to the published version of the manuscript.

Funding: This research was supported by the Office of Naval Research Global through the grant number N62909-20-1-2030.

Institutional Review Board Statement: Not applicable.

Informed Consent Statement: Not applicable.

Data Availability Statement: The data presented in this study are available on request from the corresponding author.

Acknowledgments: The authors would like to thank the Aerospace Engineering Research and Innovation Center of the Faculty of Mechanical and Electrical Engineering at the Autonomous University of Nuevo Leon and the Department of Aeronautical and Astronautical Engineering at the University of Southampton for the facilities of this research.

Conflicts of Interest: The authors declare no conflicts of interest.

References

1. Mccormick, B.W. *Aerodynamics of V/STOL Flight*; Courier Corporation: North Chelmsford, MA, USA, 1999.
2. Semotiuk, L.; Józwik, J.; Kukiełka, K.; Dziedzic, K. Design and FEM Analysis of an Unmanned Aerial Vehicle Wing. In Proceedings of the 2021 IEEE 8th International Workshop on Metrology for AeroSpace (MetroAeroSpace), Naples, Italy, 23–25 June 2021; pp. 365–370.
3. Phung, D.K.; Morin, P. Modeling and Energy Evaluation of Small Convertible UAVs. *IFAC Proc. Vol.* **2013**, *46*, 212–219. [CrossRef]
4. Greenwood, W.W.; Lynch, J.P.; Zekkos, D. Applications of UAVs in Civil Infrastructure. *J. Infrastruct. Syst.* **2019**, *25*, 04019002. [CrossRef]
5. Lozano, R. *Unmanned Aerial Vehicles Embedded Control*, 1st ed.; John Wiley-ISTE Ltd.: Hoboken, NJ, USA, 2010.
6. Aláez, D.; Olaz, X.; Prieto, M.; Villadangos, J.; Astrain, J. VTOL UAV digital twin for take-off, hovering and landing in different wind conditions. *Simul. Model. Pract. Theory* **2023**, *123*, 102703. [CrossRef]
7. Lu, K.; Liu, C.; Li, C.; Chen, R. Flight Dynamics Modeling and Dynamic Stability Analysis of Tilt-Rotor Aircraft. *Int. J. Aerosp. Eng.* **2019**, *2019*, 5737212. [CrossRef]
8. Liu, N.; Wang, Y.; Zhao, J.; Cheng, X.; He, X.; Wu, K. A new inclining flight mode and oblique takeoff technique for a tiltrotor aircraft. *Aerosp. Sci. Technol.* **2023**, *139*, 108370. [CrossRef]
9. Bautista, J.A.; Osorio, A.; Lozano, R. Modeling and Analysis of a Tricopter/Flying-Wing Convertible UAV with Tilt-Rotors. In Proceedings of the International Conference on Unmanned Aircraft Systems, Miami, FL, USA, 13–16 June 2017.
10. Chamola, V.; Kotesh, P.; Agarwal, A.; Naren.; Gupta, N.; Guizani, M. A Comprehensive Review of Unmanned Aerial Vehicle Attacks and Neutralization Techniques. *Ad Hoc Netw.* **2021**, *111*, 102324. [CrossRef] [PubMed]
11. Ducard, G.J.; Allenspach, M. Review of designs and flight control techniques of hybrid and convertible VTOL UAVs. *Aerosp. Sci. Technol.* **2021**, *118*, 107035. [CrossRef]

12. Flores, G.; Escareno, J.; Lozano, R.; Salazar, S. Quad-Tilting Rotor Convertible MAV : Modeling and Real-time Hover Flight Control. *J. Intell. Robot. Syst.* **2012**, *65*, 457–471. [CrossRef]
13. de Oliveira, T.L.; Anglade, A.; Hamel, T.; Samson, C. Control of convertible UAV with vectorized thrust. *IFAC-PapersOnLine* **2023**, *56*, 9288–9293. [CrossRef]
14. Bronz, M.; Smeur, E.J.; de Marina, H.G.; Hattenberger, G. *Development of A Fixed-Wing mini UAV with Transitioning Flight Capability*; American Institute of Aeronautics and Astronautics: Reston, VA, USA, 2017.
15. Goh, G.; Agarwala, S.; Goh, G.; Dikshit, V.; Sing, S.; Yeong, W. Additive manufacturing in unmanned aerial vehicles (UAVs): Challenges and potential. *Aerosp. Sci. Technol.* **2017**, *63*, 140–151. [CrossRef]
16. Moon, S.K.; Tan, Y.E.; Hwang, J.; Yoon, Y.J. Application of 3D printing technology for designing light-weight unmanned aerial vehicle wing structures. *Int. J. Precis. Eng. Manuf.-Green Technol.* **2014**, *1*, 223–228. [CrossRef]
17. Yanguo, S.; Huanjin, W. Design of Flight Control System for a Small Unmanned Tilt Rotor Aircraft. *Chin. J. Aeronaut.* **2009**, *22*, 250–256. [CrossRef]
18. Hassanalian, M.; Salazar, R.; Abdelkefi, A. Conceptual design and optimization of a tilt-rotor micro air vehicle. *Chin. J. Aeronaut.* **2019**, *32*, 369–381. [CrossRef]
19. He, C.; Chen, G.; Sun, X.; Li, S.; Li, Y. Geometrically compatible integrated design method for conformal rotor and nacelle of distributed propulsion tilt-wing UAV. *Chin. J. Aeronaut.* **2023**, *36*, 229–245. [CrossRef]
20. Sanchez, A.; Escareño, J.; Garcia, O.; Lozano, R. Autonomous Hovering of a Noncyclic Tiltrotor UAV: Modeling, Control and Implementation. *IFAC Proc. Vol.* **2008**, *41*, 803–808. [CrossRef]
21. D'Amato, E.; Di Francesco, G.; Notaro, I.; Tartaglione, G.; Mattei, M. Nonlinear Dynamic Inversion and Neural Networks for a Tilt Tri-Rotor UAV. *IFAC-PapersOnLine* **2015**, *48*, 162–167. [CrossRef]
22. Campos, J.M.; Cardoso, D.N.; Raffo, G.V. Robust Adaptive Control with Reduced Conservatism for a Convertible UAV. *IFAC-PapersOnLine* **2023**, *56*, 4520–4526. [CrossRef]
23. Bauersfeld, L.; Spannagl, L.; Ducard, G.J.J.; Onder, C.H. MPC Flight Control for a Tilt-Rotor VTOL Aircraft. *IEEE Trans. Aerosp. Electron. Syst.* **2021**, *57*, 2395–2409. [CrossRef]
24. Wang, H.; Sun, W.; Zhao, C.; Zhang, S.; Han, J. Dynamic Modeling and Control for Tilt-Rotor UAV Based on 3D Flow Field Transient CFD. *Drones* **2022**, *6*, 338. [CrossRef]
25. Zhao, H.; Wang, B.; Shen, Y.; Zhang, Y.; Li, N.; Gao, Z. Development of Multimode Flight Transition Strategy for Tilt-Rotor VTOL UAVs. *Drones* **2023**, *7*, 580. [CrossRef]
26. Fayez, K.; Leng, Y.; Jardin, T.; Bronz, M.; Moschetta, J.M. *Conceptual Design for Long-Endurance Convertible Unmanned Aerial System*; American Institute of Aeronautics and Astronautics: Reston, VA, USA, 2021.
27. Carlson, S. A Hybrid Tricopter/Flying-Wing VTOL UAV. In Proceedings of the 52nd Aerospace Sciences Meeting, National Harbor, MD, USA, 13–17 January 2014.
28. Prach, A.; Kayacan, E. An MPC-based position controller for a tilt-rotor tricopter VTOL UAV. *Optim. Control. Appl. Methods* **2018**, *39*, 343–356. [CrossRef]
29. Valavanis, K.; Vachtsevanos, G. *Handbook of Unmanned Aerial Vehicles*, 1st ed.; Springer: Atlanta, GA, USA, 2015.
30. Rozvany, G. The SIMP method in topology optimization—Theoretical background, advantages and new applications. In Proceedings of the 8th Symposium on Multidisciplinary Analysis and Optimization, Long Beach, CA, USA, 6–8 September 2000.
31. Telli, K.; Kraa, O.; Himeur, Y.; Ouamane, A.; Boumehraz, M.; Atalla, S.; Mansoor, W. A Comprehensive Review of Recent Research Trends on Unmanned Aerial Vehicles (UAVs). *Systems* **2023**, *11*, 400. [CrossRef]
32. Stengel, R. *Flight Dynamics*, 1st ed.; Princeton University Press: Princeton, NJ, USA, 2004.
33. Garcia Salazar, O.; Rojo Rodriguez, E.G.; Sanchez-Orta, A.; Saucedo Gonzalez, D.; Muñoz-Vázquez, A. Robust Geometric Navigation of a Quadrotor UAV on SE(3). *Robotica* **2019**, *38*, 1019–1040. [CrossRef]
34. Ollervides-Vazquez, E.J.; Rojo-Rodriguez, E.G.; Rojo-Rodriguez, E.U.; Cabriales-Ramirez, L.E.; Garcia-Salazar, O. Two-layer saturated PID controller for the trajectory tracking of a quadrotor UAV. In Proceedings of the 2020 International Conference on Mechatronics, Electronics and Automotive Engineering (ICMEAE), Cuernavaca, Mexico, 16–21 November, 2020; pp. 85–91.
35. Garcia, O.; Sanchez, A.; Escareño, J.; Lozano, R. Tail-sitter UAV having one tilting rotor: Modeling, Control and Real-Time Experiments. *IFAC Proc. Vol.* **2008**, *41*, 809–814. [CrossRef]

Disclaimer/Publisher's Note: The statements, opinions and data contained in all publications are solely those of the individual author(s) and contributor(s) and not of MDPI and/or the editor(s). MDPI and/or the editor(s) disclaim responsibility for any injury to people or property resulting from any ideas, methods, instructions or products referred to in the content.